Bioorganic Chemistry 57 (2014) 65–82

Contents lists available at ScienceDirect

Bioorganic Chemistry

journal homepage: www.elsevier.com/locate/bioorg

# Design, synthesis, 3D pharmacophore, QSAR, and docking studies of carboxylic acid derivatives as Histone Deacetylase inhibitors and cytotoxic agents

Mona M. Abdel-Atty [a], Nahla A. Farag [a], Shaymaa E. Kassab [b], Rabah A.T. Serya [c], Khaled A.M. Abouzid [c,*]

[a] Pharmaceutical Chemistry Department, Faculty of Pharmacy, Misr International University, Cairo 11431, Egypt
[b] Pharmaceutical Chemistry Department, Faculty of Pharmacy, Damanhur University, Damanhur, Egypt
[c] Pharmaceutical Chemistry Department, Faculty of Pharmacy, Ain Shams University, Cairo 11566, Egypt

ARTICLE INFO

*Article history:*
Received 19 May 2014
Available online 3 September 2014

*Keywords:*
Synthesis
Histone deacetylase
3D QSAR pharmacophore model
Cytotoxic activity

ABSTRACT

In this study, five series of (*E*)-6-(4-substituted phenyl)-4-oxohex-5-enoic acids **IIb–f (*E*)**, (*E*)-3-(4-(substituted)-phenyl)acrylic acids **IIIa–g (*E*)**, 4-(4-(substituted)phenylamino)-4-oxobutanoic acids **VIa**,**b**,**e**, 5-(4-(substituted)phenylamino)-5-oxopentanoic acids **VIIa**,**f** and 2-[(4-(substituted)phenyl) carbamoyl]benzoic acids **VIIIa**,**e** were designed and synthesized. Selected compounds were screened *in vitro* for their cytotoxic effect on 60 human NCI tumor cell lines. Compound **IIf (*E*)** displayed significant inhibitory activity against NCI Non-Small Cell Lung A549/ATCC Cancer cell line (68% inhibition) and NCI-H460 Cancer cell line (66% inhibition). Moreover, the final compounds were evaluated *in vitro* for their cytotoxic activity on HepG2 Cancer cell line in which histone deacetylase (HDAC) is overexpressed. Compounds **IIc (*E*)**, **IIf (*E*)**, **IIIb (*E*)**, and **IIIg (*E*)** exhibited the highest cytotoxic activity against HepG2 human cancer cell lines with $IC_{50}$ ranging from 2.27 to 10.71 μM. In addition, selected compounds were tested on histone deacetylase isoforms (HDAC1–11). Molecular docking simulation was also carried out for HDLP enzyme to investigate their HDAC binding affinity. In addition, generation of 3D-pharmacophore model and quantitative structure activity relationship (QSAR) models were combined to explore the structural requirements controlling the observed cytotoxic properties.



## 1. Introduction

Histone acetylation has been shown to be one of the major regulatory mechanisms for gene expression [1]. Control of expression is dependent on the balance between the competing activities of histone acetyl transferases (HATs) and histone deacetylases (HDACs) on the regulation of chromatin structure by acetylation of lysines on histone tails [2]. Acetylation of the N-terminal tails of lysine residues is done by HATs which removes positive charges, thereby reducing the affinity between histones and negatively charged DNA. This facilitates access of the transcriptional machinery to the DNA template [3]. Conversely, HDACs remove the acetyl group from the histone tails, reversing the effects of HATs and altering transcription. In general, acetylation is associated with a transcriptionally active state and deacetylation with gene silencing [4,5]. Studies demonstrated that these two enzymes are not only involved in the regulation of chromatin structure and gene expression, but they can also regulate cell-cycle progression and carcinogenic process [6]. HDACs therefore play a pivotal role in the regulation of gene expression, cell growth and proliferation [7]. Over expression of HDACs has been linked to the development of cancers in human [8]. Eighteen mammalian HDACs have been identified and categorized into four structural and functionally distinct classes [9]. Class I (HDAC1–3 and 8), class II (HDAC4–7, 9 and 10) and class IV (HDAC11). HDACs share conserved residues in the catalytic core regions and require zinc ion for deacetylation, while class III (SIRT1–7) HDACs are unrelated sirtuin deacetylases and require $NAD^+$ for their enzymatic activity [9,10].

HDAC inhibitors present a promising class of anticancer agents [11,12]. HDAC inhibition induces transcriptional events involved in growth arrest, cell proliferation, and apoptosis [13]. There are numbers of HDACIs emerging as an exciting novel class of antitumor agents as shown in Fig. 1, Trichostatin A (TSA) is an effective natural hydroxamate HDACI and suberoylanilide hydroxamic acid (Vorinostat, SAHA) is the first HDACI approved by FDA in 2006 [14–16]. Belinostat and Panobinostat are also hydroxamate HDACIs

* Corresponding author.
*E-mail address:* abouzid@yahoo.com (K.A.M. Abouzid).

http://dx.doi.org/10.1016/j.bioorg.2014.08.006
0045-2068/

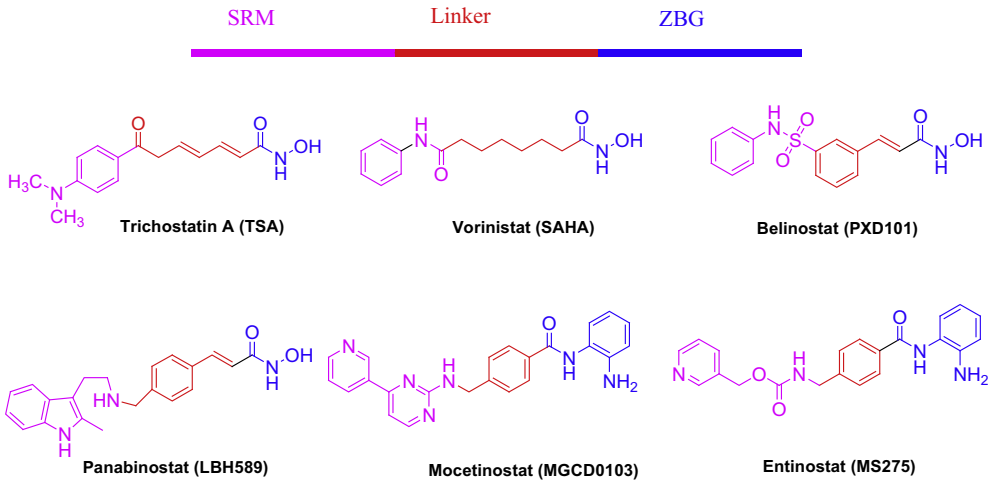


**Fig. 1.** Examples of histone deacetylase inhibitors as antitumor agents and the three essential pharmacophore features shown in color codes.

which induce acetylation of histone at nanomolar concentrations [17]. Mocetinostat and Entinostat are benzamide HDACIs with limited cardiac toxicity in preclinical studies [18].

During the past 15 years, a number of structurally diverse HDAC inhibitors have been identified which can be divided into structural classes including hydroxamates, cyclic peptides, benzamides, electrophilic ketones and carboxylic acids [19,20]. Despite their different chemical structures, these agents have a common pharmacophore composed of three portions: (a) zinc binding group (ZBG), which chelates zinc ion at the bottom of pocket, (b) linker (scaffold), usually hydrophobic which occupies the narrow channel, (c) surface recognition moiety (SRM), which interacts with hydrophobic interactions with residues on the rim of active site (Fig. 1) [21,22]. The common linkers are aliphatic chain, aromatic chain and vinyl-aromatic chain [21]. Any HDACI with its strong ZBG can substitute the native substrate and preserve the 'His-Asp' charge transfer system within the enzyme complex [23]. This 'three-component' structural template has been widely realized as a successful strategy for the design of efficient new HDACI's [24–26].

Although hydroxamic acid derivatives from the class of HDAC inhibitors is effective in nanomolar dose (TSA IC50: 12 nM and SAHA IC50: 110–370 nM) [27,28], it has problems such as poor pharmacokinetic properties, severe toxicities and non-selectivity [29]. The carboxylic acid class is the least investigated inhibitor group probably due to poor HDAC inhibition activity [19,22]. The carboxylic acid group is thought to be a metal-binding functional group [28]. A limited number of compounds such as VPA (valproic acid), BA (butyric acid) and PBA (phenyl butyric acid) are identified as carboxylic acid class HDAC inhibitors (Fig. 2) [30]. All these inhibitors are in phase trials with high micromolar doses, where they have anti-proliferative, anti-cancer and anti-convulsant effects, and their toxicity studies have been completed [31,32]. They are used for treatment of cancer and also neurodegenerative diseases such as spinal muscular atrophy (SMA) [33]. Most carboxylic acids reported to date have simple alkyl chains and the structure activity relationship studies for this group have been very limited. Therefore, advances are needed in designing new carboxylic acid derivatives with improved HDAC inhibition activity.

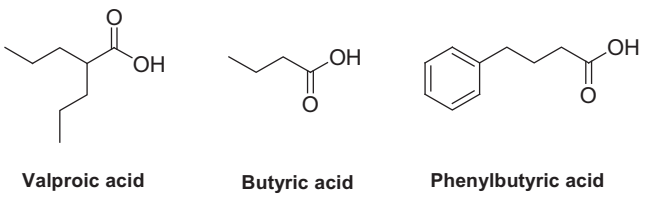


**Fig. 2.** Examples of carboxylic acids based histone deacetylase inhibitors.

## 2. Rational and design

The design of the newly synthesized compounds was based on earlier study of carboxylic acid as zinc binding functional group in histone deacetylase metallo-enzymes [28], directing the design toward the synthesis of carboxylic acid derivatives as HDAC inhibitors in an attempt to increase their potency by manipulating the carboxylic acid moiety as zinc binding group to be directly attached to the linker ($n = 0$) as in series **III** or expand the chain ($n = 2, 3$) as in series **II**, **VI**, **VII** or rigidify the side chain through incorporation of phenyl moiety as in series **VIII**. In addition, modifying the SRM to be heterocyclic or aromatic amine derivatives which are essential for recognizing and binding to the rim of the active pocket of the HDAC enzymes and also developing the hydrocarbon linker which occupies the hydrophobic channel with styrene as in series **II**, **III** or benzamide as in series **VI**, **VII**, **VIII** which are approaches to enrich and optimize HDAC inhibition activity [21], as shown in Fig. 3.

Design of the target compounds was based on molecular docking study which was carried out on X-ray crystal structure of HDLP enzyme (histone deacetylase like protein) PDB code (1C3S) complexed with its binding inhibitor SAHA (suberoylanilide hydroxamic acid) to predict the binding affinities and orientation of the target compounds at the active site of HDAC. In addition, we describe the structural requirements and structure–activity relationships on carboxylic acid derivatives as cytotoxic agents by successfully generating a valid 3D-pharmacophore model which was then combined to generate a validated 2D-QSAR model to explore the structural requirements controlling the observed cytotoxic activity estimated by the effect of the synthesized compounds on HepG2 Cancer cell line.

Selected compounds were evaluated for their cytotoxic effect on sixty human tumor cell lines, under the drug discovery program of the NCI and their enzyme inhibitory effect on different HDAC isoforms. Target compounds were also *in vitro* tested for their cytotoxic effect on Liver HepG2 Cancer cell line.

## 3. Chemistry

The route adopted for the synthesis of the novel (*E*)-6-(4-(substituted)phenyl)-4-oxohex-5-enoic acids **IIb–f (*E*)** and (*E*)-3-(4-(substituted)phenyl)-acrylic acids **IIIa–g (*E*)** is depicted in Scheme 1.

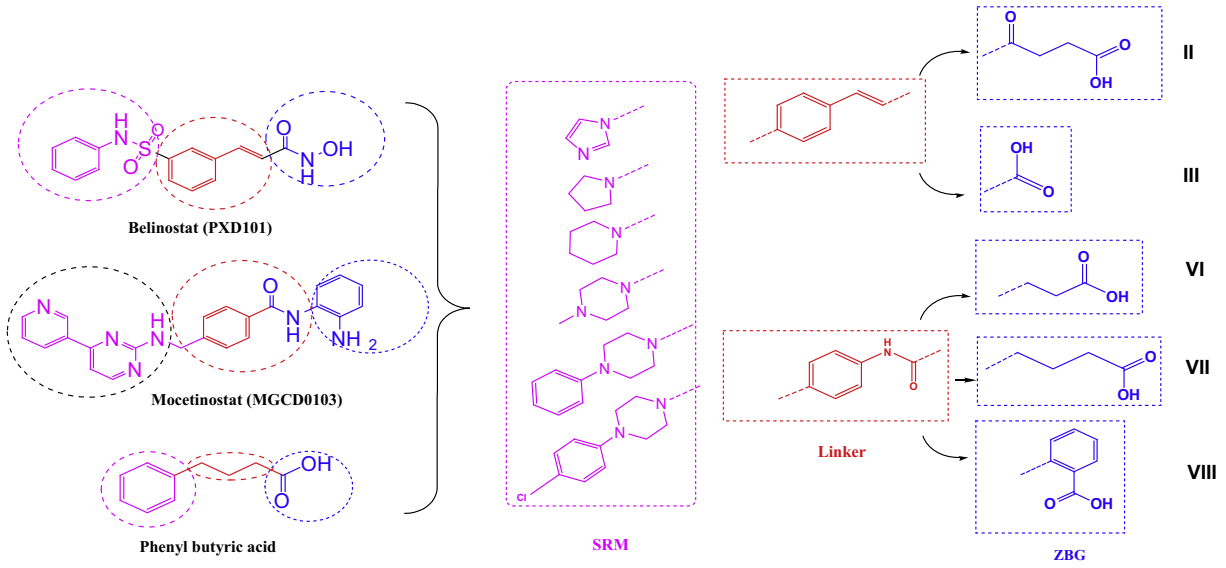


**Fig. 3.** Design strategy and structures of target compounds.

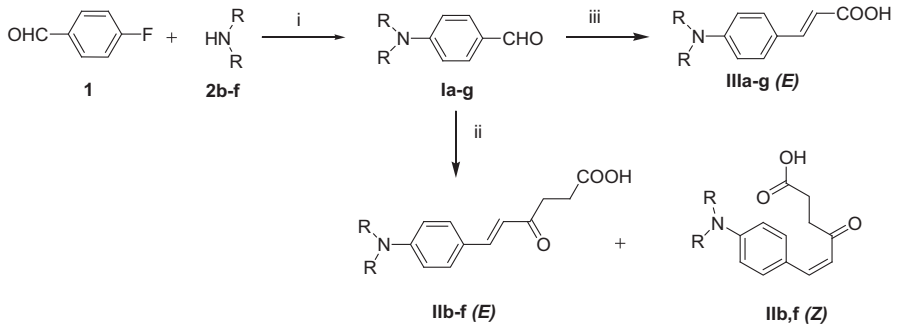


**Scheme 1.** Synthesis of (*E*)-6-(4-(substituted)phenyl)-4-oxohex-5-enoic acids **IIb–f (*E*)**, (*Z*)-6-(4-(substituted)phenyl)-4-oxohex-5-enoic Acids **IIb,f (*Z*)** and (*E*)-3-(4-(substituted)phenyl)acrylic acids **IIIa–g (*E*)**. Reagents and conditions: (i) potassium carbonate, Aliquat 336 in dimethylformamide, reflux, 24 h. (ii) Levulinic acid, piperidine and acetic acid in benzene, reflux, 6 h. (iii) Malonic acid, piperidine in pyridine, reflux, 4 h.

The key intermediate 4-(substituted) benzaldehyde derivatives **Ia–g** were prepared following the literature methods as illustrated in Scheme 1 [34]. 4-(Substituted) benzaldehyde derivatives **Ia–g** were synthesized in good yield through the reaction of p-fluorobenzaldehyde **1** with the appropriate amine **2a–g** using potassium carbonate and Aliquat 336 as a catalyst mixed in dimethylformamide (DMF) under reflux affording the corresponding benzaldehydes **Ia–g**. (*E*)-6-(4-(substituted)phenyl)-4-oxohex-5-enoic acids **IIb–f (*E*)** were prepared by the condensation of the appropriate aldehyde **Ib–f** and levulinic acid using catalytic amounts of piperidine and acetic acid in benzene under reflux, with azeotropic removal of water using a DeanStark trap [35] to give novel hexenoic acid derivatives **IIb–f (*E*)** as presented in Scheme 1. Under these conditions, the carbanion formed at the α-methyl group of levulinic acid adds to the aldehyde carbon followed by dehydration to afford the arylidine ketoacid derivatives **IIb–f (*E*)**. $^1$H NMR shows the formation of *E*-isomers with minor amounts of *Z*-isomers which were detected by TLC as minor spots that are removed upon recrystallization from the given solvent. Exceptionally, during synthesis of hexenoic acid derivatives **IIb (*E*)** and **IIf (*E*)**, the appropriate *Z*-isomers were obtained in good yields with their *E*-isomers and were separated by column chromatography using hexane/ethyl acetate 8:2 as the elution system for separation to produce the pure (*E*)-6-(4-(pyrrolidin-1-yl)phenyl)-4-oxo-hex-5-enoic acid **IIb (*E*)**, (*Z*)-6-(4-(pyrrolidin-1-yl)phenyl)-4-oxo-hex-5-enoic acid **IIb (*Z*)**, (*E*)-6-(4-(4-phenylpiperazin-1-yl)phenyl)-4-oxohex-5-enoic acid **IIf (*E*)** and (*Z*)-6-(4-(4-phenylpiperazin-1-yl)phenyl)-4-oxohex-5-enoic acid **IIf (*Z*)**.

Compound **IIb (*E*)** was confirmed as an *E*-isomer by $^1$H NMR, where the spectrum of its *E*-isomer revealed coupling constants of —CH=CH— higher than that of its *Z*-isomer. $^1$H NMR spectrum of **IIb (*E*)** revealed a doublet signal with an integration of one proton —CH=CH—CO at δ6.56–6.62 ppm (1H) with $J$ = 16.2 Hz which was coupled with the other proton —CH=CH—CO appearing as doublet signal at δ7.56–7.61 ppm (1H) with $J$ = 15.9 Hz, while compound **IIb (*Z*)** was confirmed as a *Z*-isomer by $^1$H NMR spectrum where —CH=CH—CO appeared as doublet signal at δ6.56–6.62 ppm (1H) with $J$ = 8 Hz which was coupled with —CH=CH—CO appearing as doublet signal at δ7.52–7.54 ppm (1H) with $J$ = 8 Hz. Similarly compound **IIf (*E*)** was confirmed as an *E*-isomer by $^1$H

NMR spectrum, where the coupling constants of —CH=CH— where higher than its *Z* isomer. $^1$H NMR of —CH=CH—CO appeared as doublet signal at δ6.61–6.66 ppm (1H) with *J* = 16.2 Hz which was coupled with —CH=CH—CO appearing as doublet at δ7.53–7.58 ppm (1H) with *J* = 16.2 Hz, while compound **IIf (*Z*)** was confirmed as a *Z*-isomer by $^1$H NMR where —CH=CH—CO appeared as singlet signal at δ6.82 ppm (1H) and CH=CH—CO appearing as doublet signal at δ7.52–7.54 (1H) with *J* = 6.4 Hz.

(*E*)-3-(4-(Substituted)-phenyl)acrylic acids **IIIa–g (*E*)** were prepared by mixing of the appropriate aldehyde **Ia–g** and malonic acid in pyridine under reflux using catalytic amount of piperidine as presented in Scheme 1. *E*-isomers were obtained as a sole product and confirmed by $^1$H NMR where the coupling constant of —CH=CH—COOH appeared as doublet at δ6.20–6.40 ppm (1H) with *J* = 16.2 Hz which was coupled with —CH=CH—COOH appearing as doublet at δ7.40–7.60 (1H) with *J* = 16.2 Hz.

The pathway applied for the synthesis of 4-(4-(substituted)phenylamino)-4-oxobutanoic acids **VIa**,**b**,**e**, 5-(4-(substituted)-phenylamino)-5-oxopentanoic acids **VIIa**,**f** and 2-((4-substituted)phenyl) carbamoyl)benzoic acids **VIIIa**,**e** were presented in Scheme 2. The key intermediates 4-(substituted) aniline **Va**,**b**,**e**,**f** were prepared following the literature methods [36,37], where 1-(amino substituted)-4-nitrobenzene **IVa**,**b**,**e**,**f** were synthesized through the reaction of para nitro chlorobenzene **3** with the appropriate amine **2a**,**b**,**e**,**f** using potassium carbonate and Aliquat 336 as a catalyst mixed in dimethyl formamide under reflux affording 1(amino substituted) 4-nitrobenzene **IVa**,**b**,**e**,**f**. Reduction of the synthesized nitro derivatives **IVa**,**b**,**e**,**f** to their amino derivatives using sodium dithionite in ammonia to yield the corresponding intermediate 4-(substituted) aniline **Va**,**b**,**e**,**f**. Finally stirring of 4(substituted) aniline **Va**,**b**,**e**,**f** with the appropriate anhydride (succinic anhydride, glutaric anhydride and phthalic anhydride) in methylene chloride at room temperature afforded 4-(4-(substituted)phenylamino)-4-oxobutanoic acids **VIa**,**b**,**e**, 5-(4-(substituted)phenylamino)-5-oxopentanoic acids **VIIa**,**f**, and 2-((4-substituted)phenyl)carbamoyl) benzoic acids **VIIIa**,**e**, respectively.

## 4. Results and discussion

### 4.1. Biological evaluation

#### 4.1.1. In vitro anticancer activity

*4.1.1.1. Primary single dose ($10^{-5}$ M) full NCI 60 cell panel in vitro assay.* Ten structures of the final carboxylic acid based products were submitted to National Cancer Institute "NCI" (www.dtp.nci.nih.gov), Bethesda, Maryland, USA, and eight compounds were selected on the basis of degree of structure variation and computer modeling techniques for evaluation of their antineoplastic activity. The tumor growth inhibition properties of the eight compounds **IIb–f (*E*)**, **IIIf (*E*)**, **VIb** and **VIIf** with their respective NCI codes: NSC D-780150/1, NSC D-780151/1, NSC D-780154/1-, NSC D-780152/1, NSC D-780153/1, NSC D-780155/1, NSC D-780157/1 and NSC D-780156/1, were selected among the synthesized compounds **IIb–f (*E*)**, **IIIb**,**c**,**f**, **VIb**, **VIIf** by the National Cancer Institute (NCI), USA and were screened on human tumor cell lines, under the drug discovery program of the NCI.

Primary *in vitro* one dose ($10^{-5}$ M concentration) anticancer assay was performed in full NCI 60 cell panel. Results for each compound were reported as a mean graph of the percent growth of the treated cells when compared to the untreated control cells. Analysis of historical Development Therapeutics Programme (DTP) was performed and results are represented in Table 1.

Compounds **IIf (*E*)** and **IIIf (*E*)** among the tested compounds showed selectivity and sensitivity against different NCI cell panel.

In series **II**, compound **IIf (*E*)** showed remarkably lowest cell growth promotion against Non-Small Cell Lung A549/ATCC Cancer cell line (cell growth promotion 32%, inhibition 68%) and NCI-H460 Cancer cell line (cell growth promotion 34%, inhibition 66%). Also it exhibited broad spectrum cell growth inhibition against Leukemia SR Cancer cell line (cell growth promotion 44.38%, inhibition 55.62%), K-562 Cancer cell line (cell growth promotion 65.61%, inhibition 34.39%), Breast T-47D Cancer cell line (cell growth promotion 75.68%, inhibition 24.32%), Non-Small Cell Lung NCI-H23

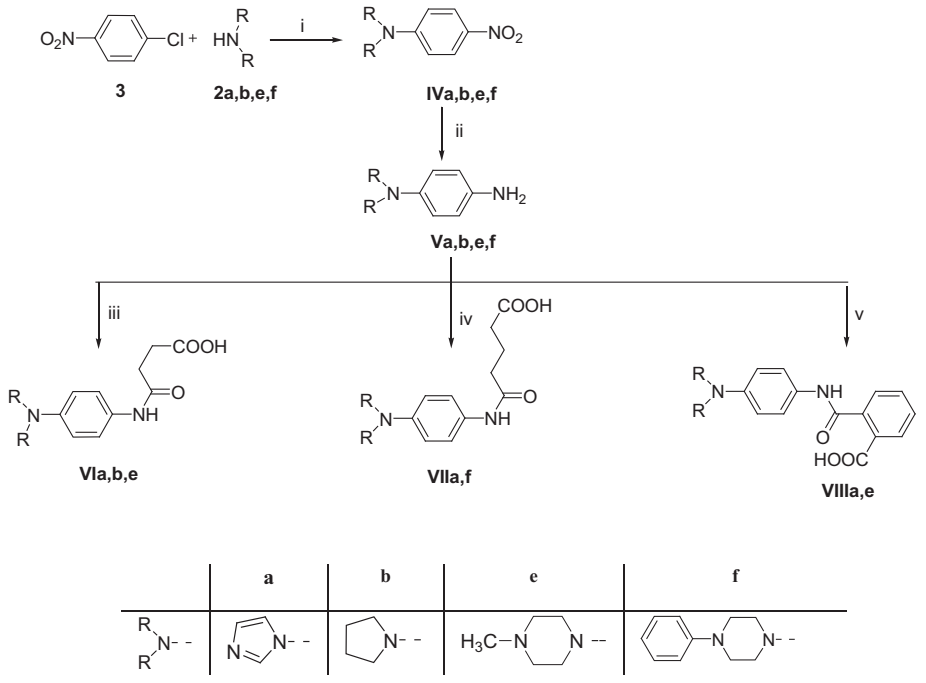


**Scheme 2.** Synthesis of 4-(4-(substituted)phenylamino)-4-oxobutanoic acids **VIa**,**b**,**e**, 5-(4-(substituted)phenylamino)-5-oxopentanoic acids **VIIa**,**f** and 2-((4-substituted)phenyl)carbamoyl)benzoic acids **VIIIa–e**. Reagents and conditions: (i) potassium carbonate, Aliquat 336 in dimethylformamide, reflux, 24 h. (ii) Sodium dithionite in ammonia, reflux, 6 h. (iii) Succinic anhydride in methylene chloride, stir at room temperature. (iv) Glutaric anhydride in methylene chloride, stir at room temperature. (v) Phthalic anhydride in methylene chloride, stir at room temperature.

**Table 1**
Sixty human tumor cell line anticancer screening data at single dose assay ($10^{-5}$ M concentration) as percent cell growth promotion of **IIb–f (*E*)**, **IIIf (*E*)**, **VIb**, **VIIf**.

| | IIb (*E*) | IIc (*E*) | IId (*E*) | IIe (*E*) | IIf (*E*) | IIIf (*E*) | VIb | VIIf |
|---|---|---|---|---|---|---|---|---|
| *Leukemia* | | | | | | | | |
| CCRF-CEM | **89.13** | **81.60** | 97.30 | 95.52 | **86.34** | 98.34 | 98.77 | 113.81 |
| HL-60(TB) | 94.03 | 77.66 | 97.58 | 101.86 | **81.41** | 96.78 | 96.63 | 97.89 |
| K-562 | 93.17 | 72.14 | 92.03 | **82.67** | 65.61 | 95.20 | 92.23 | 96.64 |
| MOLT-4 | 91.73 | **80.57** | 95.50 | 92.88 | **84.32** | **86.96** | 100.62 | 99.81 |
| RPMI-8226 | 95.12 | 92.58 | 101.79 | 95.69 | 90.76 | 95.16 | 106.09 | 103.14 |
| SR | 107.76 | 79.02 | 103.18 | 98.14 | 44.38 | **81.99** | 103.70 | 98.17 |
| *Non-Small Cell Lung Cancer* | | | | | | | | |
| A549/ATCC | 93.88 | 90.22 | 90.92 | 98.09 | 32.24 | 99.76 | 98.62 | 103.57 |
| HOP-62 | 100.21 | 93.66 | 108.32 | 99.48 | 95.65 | 92.29 | 101.27 | 97.30 |
| HOP-92 | 92.08 | **81.93** | 97.38 | 91.20 | 83.75 | **89.75** | 103.12 | 105.53 |
| NCI-H226 | 91.39 | 95.21 | 97.91 | 99.97 | 83.73 | 73.05 | 98.85 | 102.24 |
| NCI-H23 | 93.60 | **87.90** | 97.77 | 98.85 | 77.60 | 97.35 | 99.78 | 97.79 |
| NCI-H322M | 101.29 | 97.35 | 96.15 | 102.97 | 82.41 | 91.99 | 111.91 | 111.03 |
| NCI-H460 | 105.08 | 103.95 | 102.79 | 108.55 | 34.23 | 102.50 | 106.22 | 104.08 |
| NCI-H522 | **86.95** | **82.81** | 96.06 | 96.39 | **86.85** | **82.01** | 103.33 | 96.00 |
| *Colon Cancer* | | | | | | | | |
| COLO 205 | 116.44 | 105.42 | 115.18 | 110.00 | 113.98 | 116.74 | 107.53 | 104.05 |
| HCC-2998 | 90.57 | 94.10 | **85.84** | 100.11 | **84.64** | 106.23 | 111.41 | 100.29 |
| HCT-116 | 93.80 | **85.31** | 92.97 | 103.48 | **80.56** | **86.84** | 101.56 | 103.85 |
| HCT-15 | 108.64 | 101.66 | 102.95 | 103.69 | **87.37** | 103.19 | 99.41 | 94.90 |
| HT29 | **85.70** | **89.58** | 99.79 | 102.37 | 94.59 | 100.78 | 107.90 | 104.30 |
| KM12 | 100.85 | 99.22 | 103.65 | 104.48 | 95.08 | 102.94 | 104.42 | 106.92 |
| SW-620 | 101.15 | 98.20 | 107.87 | 103.26 | 102.80 | 103.69 | 104.18 | 98.51 |
| *CNS Cancer* | | | | | | | | |
| SF-268 | 91.19 | 95.60 | 98.41 | 102.78 | 107.93 | 103.58 | 108.91 | 99.70 |
| SF-295 | 111.04 | 99.70 | 103.99 | 105.74 | 77.80 | 100.61 | 99.17 | 94.90 |
| SF-539 | 104.24 | 103.57 | 95.58 | 102.50 | 106.95 | 99.37 | 101.16 | 94.06 |
| SNB-19 | 101.18 | 101.61 | 107.29 | 103.15 | 103.85 | 109.28 | 107.95 | 107.91 |
| SNB-75 | 107.51 | 97.69 | 96.55 | 92.04 | 107.80 | 106.83 | **83.02** | **80.89** |
| U251 | 88.17 | **87.51** | 94.56 | 100.31 | **86.26** | **88.50** | 104.93 | 102.63 |
| *Melanoma* | | | | | | | | |
| LOX IMVI | 94.74 | 94.28 | 97.10 | 99.56 | 91.78 | **87.87** | 100.81 | 96.99 |
| MALME-3M | 105.59 | 96.11 | 96.47 | 90.33 | 89.14 | 91.37 | 107.02 | 100.54 |
| M14 | 97.37 | 97.42 | 92.80 | 101.54 | 102.53 | 105.10 | 99.85 | 104.41 |
| MDA-MB-435 | 103.72 | 110.11 | 112.05 | 109.23 | 101.79 | 112.86 | 106.30 | 103.68 |
| SK-MEL-2 | 105.23 | 103.83 | 101.13 | 102.70 | 96.41 | 110.19 | 111.07 | 105.88 |
| SK-MEL-28 | 107.18 | 103.61 | 100.66 | 107.25 | 101.35 | 111.91 | 101.69 | 101.72 |
| SK-MEL-5 | 97.61 | 95.91 | 100.35 | 102.06 | 98.83 | 93.89 | 100.25 | 104.07 |
| UACC-257 | **84.00** | **88.73** | 90.69 | 92.40 | 90.66 | 79.21 | 96.91 | 101.16 |
| UACC-62 | 91.26 | 91.07 | 104.22 | 99.41 | **88.34** | 97.80 | 111.37 | 102.69 |
| *Ovarian Cancer* | | | | | | | | |
| IGROV1 | 98.36 | 91.31 | 103.69 | 104.87 | 106.13 | 96.60 | 109.23 | 113.88 |
| OVCAR-3 | 97.94 | 97.29 | 101.20 | 110.76 | 99.33 | 102.98 | 108.74 | 105.96 |
| OVCAR-4 | 98.00 | 104.46 | 110.24 | 108.94 | 97.49 | 118.31 | 101.36 | 96.74 |
| OVCAR-5 | 103.04 | 97.62 | 94.43 | 104.46 | 114.57 | 78.16 | 102.86 | 102.59 |
| OVCAR-8 | 97.91 | **89.90** | 101.77 | 102.14 | 96.72 | 100.41 | 101.46 | 110.34 |
| NCI/ADR-RES | 97.49 | 98.54 | 102.70 | 103.53 | 92.91 | 100.91 | 105.39 | 100.86 |
| SK-OV-3 | 108.7 | 98.50 | 116.30 | 101.52 | 94.86 | 112.15 | 108.27 | 111.43 |
| *Renal Cancer* | | | | | | | | |
| 786-0 | 99.06 | 98.70 | 96.35 | 94.90 | 92.22 | **87.80** | 93.23 | 99.29 |
| ACHN | 105.01 | 100.75 | 109.65 | 109.71 | 107.98 | 109.98 | 106.95 | 100.30 |
| CAKI-1 | 101.03 | 107.18 | 104.19 | 108.13 | 105.26 | 110.43 | 91.52 | 94.33 |
| RXF 393 | 95.96 | 106.10 | 115.14 | 107.29 | 114.99 | 92.21 | 106.75 | 104.71 |
| SN12C | 101.09 | 97.76 | 106.06 | 99.89 | 98.11 | 106.33 | 105.33 | 104.38 |
| TK-10 | 104.65 | 100.25 | 99.13 | 95.82 | 91.97 | 93.80 | 107.24 | 107.41 |
| UO-31 | **88.54** | **84.50** | **86.56** | 95.05 | 90.71 | **89.23** | 101.66 | 94.30 |
| *Prostate Cancer* | | | | | | | | |
| PC-3 | 94.10 | **89.51** | 97.88 | 99.49 | **87.52** | 101.75 | 97.11 | 102.26 |
| DU-145 | 94.92 | 95.64 | 109.30 | 105.09 | 94.75 | 101.80 | 109.07 | 109.53 |
| *Breast Cancer* | | | | | | | | |
| MCF7 | 99.69 | **88.17** | 95.55 | 99.07 | **80.56** | **86.51** | 96.10 | **89.28** |
| MDA-MB 231/ATCC | 106.10 | **88.23** | 110.81 | 103.34 | 98.70 | 103.17 | 113.92 | 109.55 |
| HS 578T | 100.67 | 100.21 | 104.72 | 105.59 | 105.52 | 109.41 | 102.28 | 100.17 |
| BT-549 | **85.01** | **88.83** | 100.03 | 99.14 | 96.45 | **88.90** | 102.40 | 98.74 |
| T-47D | 76.60 | 61.28 | 100.53 | 94.68 | 75.68 | 74.03 | 103.93 | 106.87 |
| MDA-MB-468 | 96.70 | 101.29 | 102.91 | 95.99 | **87.29** | 42.66 | 103.33 | 104.53 |

**O** 10-20% growth inhibition, **O** 20-30% growth inhibition, **O** 30-40% growth inhibition, **O** 50-60% growth inhibition, **O** 60-70% growth inhibition

Cancer cell line (cell growth promotion 77.6%, inhibition 22.4%). Compound **IIc (*E*)** is the second active compound from series **II**, it was found to be active mostly against breast cancer T-47D cell line (cell growth promotion 61.28%, inhibition 38.72%). Compound **IIc (*E*)** showed inhibition activity also against Leukemia HL-60(TB) (cell growth promotion 77.66%, inhibition 22.34%) and K-562 (cell growth promotion 72.14%, inhibition 27.86%) cancer cell lines. Compound **IIb (*E*)** showed lower inhibition activity, where it shows activity mostly against Breast T-47D Cancer cell line (cell growth promotion 76.6%, inhibition 23.4%). Compounds **IId (*E*)** and **IIe (*E*)** showed lowest inhibition activity among the tested series **II** compounds.

In series **III**, compound **IIIf (*E*)** was found to be most active against Breast cancer MDA-MB-468 cell line (cell growth promotion 42.66%, inhibition 57.34%). Compound **IIIf (*E*)** showed broad spectrum of inhibition activity against Non-Small Lung Cancer NCI-H226 cell line (cell growth promotion 73.05%, inhibition 26.95%), Breast cancer T-47D cell line (cell growth promotion

**Table 2**
Data of the *in vitro* anticancer activity on HepG2 Cancer cell line.

| Test compound | $IC_{50}$[a] (μM) |
|---|---|
| **IIb (*E*)** | 63.58 |
| **IIb (*Z*)** | 413.9 |
| **IIc (*E*)** | *2.27* |
| **IId (*E*)** | 138.1 |
| **IIe (*E*)** | 904.8 |
| **IIf (*E*)** | *10.21* |
| **IIf (*Z*)** | 849.2 |
| **IIIa (*E*)** | 21.02 |
| **IIIb (*E*)** | *10.71* |
| **IIIc (*E*)** | *18.04* |
| **IIId (*E*)** | 45.69 |
| **IIIe (*E*)** | 430.7 |
| **IIIf (*E*)** | 32.85 |
| **IIIg (*E*)** | *10.63* |
| **VIa** | 468.2 |
| **VIb** | 997.2 |
| **VIe** | 672.7 |
| **VIIa** | 629.5 |
| **VIIf** | 725.2 |
| **VIIIa** | 548.1 |
| **VIIIe** | 525.7 |
| SAHA | 63.48[39] |

[a] $IC_{50}$ value is the compound concentration required to produce 50% inhibition of HepG2 human liver cancer cell line.

74.03%, inhibition 25.96%), ovarian cancer OV-CAR8 cell line (cell growth promotion 78.16%, inhibition 21.84%) and Melanoma UACC-257 cell line (cell growth promotion 79.21%, inhibition 20.79%).

While in series **VI** and **VII**, compounds **VIb** and **VIIf** showed insignificant activity against most of the 60 tested cancer cell lines.

*4.1.1.2. In vitro cytotoxicity assay on HepG2 human liver cancer cell line.* Furthermore, 21 synthesized compounds were evaluated for their cytotoxic activity on human liver cancer cell line HepG2 in which HDAC1 is over expressed [38]. Cytotoxicity assay on HepG2 Cancer cell line was determined using sulforhodamine B assay method (SRB). The concentration of the test compounds causing 50% inhibition ($IC_{50}$, μM) was calculated from the concentration–inhibition response curve (triplet determinations) and are represented in Table 2.

In series **II** and series **III**, it was found that compounds **IIc (*E*)**, **IIf (*E*)**, **IIIg (*E*)**, **IIIb (*E*)** displayed potent cytotoxic activities with $IC_{50}$ values 2.27, 10.21, 10.63 and 10.71 μM respectively, comparable with SAHA having $IC_{50}$ value of 63.48 μM [39]. Compounds **IIIc (*E*)**, **IIIa (*E*)**, **IIIf (*E*)**, **IIId (*E*)**, and **IIb (*E*)** displayed significant cytotoxic activity with $IC_{50}$ values 18.04, 21.01, 32.85, 45.69 and 63.58 μM respectively. Other compounds **IId (*E*)**, **IIe (*E*)** and **IIIe (*E*)** displayed IC50 > 100 μM. While series **VI**, **VII**, and **VIII** displayed poor cytotoxic activity compared to series **II** and **III** carboxylic acids derivatives.

Interestingly compounds **IIb (*Z*)** and **IIf (*Z*)** which are representing the *Z*-isomers of 6-(4-(pyrrolidin-1-yl)phenyl)-4-oxo-hex-5-enoic acid and 6-(4-(4-phenylpiperazin-1-yl)phenyl)-4-oxohex-5-enoic acid respectively, displayed poor cytotoxic activity with $IC_{50}$ values of 413.9 and 849.2 μM respectively, compared with their *E*-isomers **IIb (*E*)** and **IIf (*E*)** with $IC_{50}$ value of 63.48 and 10.21 μM respectively.

In conclusion, it is found that series **II** and series **III** displayed significant cytotoxic activity utilizing styrene as a linker to be considered essential for its biological effect. On the other hand, insignificant cytotoxic effect was observed in series **VI**, **VII** and **VIII** carboxylic acid derivatives which utilizes benzamide as a linker. Exceptionally, compounds **IId (*E*)** ($NHR_2$ = morpholine), **IIe (*E*)** ($NHR_2$ = methylpiperazine) and **IIIe (*E*)** ($NHR_2$ = methylpiperazine) exhibited poor cytotoxic effect.

*4.1.2. In vitro HDAC enzyme inhibition assay*

Nine synthesized carboxylic acid compounds **IIb**,**c**,**f (*E*)**, **IIIb**,**f**,**g (*E*)**, **VIa**, **VIIa** and **VIIIa** were selected as representatives for the five series in the present study to be *in vitro* tested for HDAC1 enzyme inhibition. The percentage inhibition at 10 μM concentration of the synthesized compounds against HDAC1 is summarized in Table 3. Synthesized Compounds were expected to inhibit HDACs according to molecular docking study that was performed in the present study on HDAC class I homologue (HDAC-like protein, HDLP)/SAHA complex (PDB: 1C3S) which shares 35.2% sequence identity with HDAC1 [23,10]. Results show that at 10 μM concentration, none of the tested compounds showed significant inhibitory activity against HDAC1.

Further *in vitro* enzyme inhibition assay was carried out on 3 synthesized carboxylic acid compounds selected as representatives for three series presented in this study, series **II** ((4-(substituted)phenyl)-4-oxohexanoic acids), series **III** (4-(substituted) phenyl) acrylic acids) and series **VII** 5-(4-(substituted)phenylamino)-5-oxopentanoic acid to identify the series endowed with HDAC inhibitory activity on different HDAC isoforms (HDAC2–11). Compounds **IIf (*E*)**, **IIIf (*E*)** and **VIIa** were randomly selected to test their percentage inhibition at 50 μM concentration on different HDAC isoforms (2–11). The percentage inhibition of the tested compounds at 50 μM concentration is summarized in Table 4. Results show that surprisingly newly synthesized compound **IIf (*E*)** showed remarkable increase in HDAC activity against different HDAC isoforms instead of the expected inhibitory activity against

**Table 3**
The percentage inhibition of synthesized compounds at 10 μM concentration against HDAC1.

| Test compound at (10 μM) | **IIb (*E*)** | **IIc (*E*)** | **IIf (*E*)** | **IIIb (*E*)** | **IIIf (*E*)** | **IIIg (*E*)** | **VIa** | **VIIa** | **VIIIa** | SAHA (500 nM) |
|---|---|---|---|---|---|---|---|---|---|---|
| HDAC1 % Inhibition | −10 | −6 | −5 | 2 | −3 | 1 | 4 | 3 | 5 | 84 |

**Table 4**
The percentage inhibition of compounds **IIf (*E*)**, **IIIa (*E*)** and **VIIa** at 50 μM concentration against (HDAC2–11). ND: not done.

| % Inhibition at 50 μM | HDAC2 | HDAC3 | HDAC4 | HDAC5 | HDAC6 | HDAC7 | HDAC8 | HDAC9 | HDAC10 | HDAC11 |
|---|---|---|---|---|---|---|---|---|---|---|
| **IIf (*E*)** | −19 | −73 | −37 | −75 | −27 | −65 | −53 | −38 | −29 | −42 |
| **IIIf (*E*)** | 15 | 7 | 4 | 20 | 27 | 9 | 25 | −5 | 1 | −2 |
| **VIIa** | 6 | −1 | 2 | 1 | −1 | 2 | 1 | 1 | 3 | 1 |
| SAHA (500 nM) | 74 | 90 | ND | ND | 97 | ND | ND | ND | ND | ND |
| TSN (30 μM) | ND | ND | 88 | 78 | ND | 90 | 89 | 87 | 85 | 84 |

**Table 5**
Docking results for the synthesized compounds as well as SAHA in the active site of HDLP enzyme PDB (1C3S) showing the H-bonds, Pi-interactions formed with the binding site residues and also distance of atoms related to zinc metal.

| Name | $IC_{50}$ μM | CDOCKER energy | Hydrogen bonds | Hydrogen bond distance | pi–pi interactions | Distance related to zinc |
|---|---|---|---|---|---|---|
| SAHA | 63.48 | −46.07 | HE2 of HIS131 – O of OH<br>NE2 of HIS132 – H of hydroxamic NH<br>HH of TYR297 – O of amidic C=O | 2.41<br>1.9<br>1.79 | None | 1.79 (C=O, amide)<br>1.84 (OH, hydroxamic) |
| **IIb (*E*)** | 63.58 | −43.27 | HE2 of HIS131 – O of acidic C=O<br>HH of TYR297 – O of ketonic C=O<br>HN1 of GLY295 – O of acidic OH | 2.14<br>2.32<br>2.06 | PHE141 – phenyl ring of styrene<br>PHE198 – phenyl ring of styrene | 2.19 (C=O, ketonic)<br>2.27 (C=O, acidic) |
| **IIb (*Z*)** | 413.9 | −21.96 | HH of TYR297 – O of acidic OH | 2 | PHE198 – phenyl ring of styrene | 2.15 (C=O, ketonic) |
| **IIc (*E*)** | 2.27 | −51.44 | HE2 of HIS131 – O of acidic C=O<br>HH of TYR297 – O of ketonic C=O | 2.18<br>2.33 | PHE141 – phenyl ring of styrene<br>PHE198 – phenyl ring of styrene | 2.24 (C=O ketonic)<br>2.22 (C=O acidic) |
| **IId (*E*)** | 138.1 | −33.33 | O of GLY129 – H of acidic OH | 2.38 | PHE141 – phenyl ring of styrene<br>PHE198 – phenyl ring of styrene | 2.18 (OH, acidic) |
| **IIe (*E*)** | 904.8 | −43.8 | O of GLY129 – H of acidic OH | 2.14 | PHE141 – phenyl ring of styrene<br>PHE198 – phenyl ring of styrene | 2.65 (C=O, ketonic)<br>3.21 (C=O, acidic) |
| **IIf (*E*)** | 10.21 | −48.8 | HE2 of HIS131 – O of acidic C=O<br>HH of TYR297 – O of ketonic C=O | 2.14<br>2.35 | PHE141 – phenyl ring of styrene<br>PHE198 – phenyl ring of styrene | 2.21 (C=O, ketonic)<br>2.27 (C=O, acidic) |
| **IIf (*Z*)** | 849.2 | −28.4 | HH of TYR297 – O of ketonic C=O | 2.46 | PHE141 – phenyl ring of styrene<br>PHE198 – phenyl ring of styrene | 7.44 (C=O, acidic) |
| **IIIa (*E*)** | 21.02 | −28.6 | HH of TYR297 – O of acidic OH | 2.42 | PHE141 – phenyl ring of styrene<br>PHE198 – phenyl ring of styrene and imidazole ring | 1.53 (C=O, acidic)<br>2.19 (OH acidic) |
| **IIIb (*E*)** | 10.71 | −28.14 | HH of TYR297 – O of acidic C=O<br>NE2 of HIS132 – H of acidic OH | 1.84<br>2.44 | None | 2.88 (C=O, acidic)<br>1.76 (OH, acidic) |
| **IIIc (*E*)** | 18.04 | −37.68 | HH of TYR297 – O of acidic OH | 2.82 | PHE141 – phenyl ring of styrene<br>PHE198 – phenyl ring of styrene | 2.86 (C=O, acidic)<br>2.43 (OH acidic) |
| **IIId (*E*)** | 45.69 | −37.23 | HH of TYR297 – O of acidic OH | 2.94 | PHE141 – phenyl ring of styrene<br>PHE198 – phenyl ring of styrene | 2.46 (C=O, acidic)<br>1.83 (OH, acidic) |
| **IIIe (*E*)** | 430.7 | −31.14 | O of GLY140 – H of acidic OH | 2.38 | PHE141 – phenyl ring of styrene<br>PHE198 – phenyl ring of styrene | 2.14 (OH acidic) |
| **IIIf (*E*)** | 32.85 | −37.48 | HH of TYR297 – O of acidic OH | 2.38 | PHE141 – phenyl ring of styrene<br>PHE198 – phenyl ring of styrene | 2.53 (C=O, acidic)<br>2.48 (OH, acidic) |
| **IIIg (*E*)** | 10.63 | −40.02 | HH of TYR297 – O of acidic C=O<br>HE2 of HIS131 – O of acidic OH<br>NE2 of HIS132 – H of acidic OH | 2.39<br>2.43<br>2.15 | PHE198 – phenyl ring of styrene | 2.15 (C=O, acidic)<br>2.64 (OH, acidic) |
| **VIa** | 468.2 | −30.35 | O of GLY140:O – H of acidic OH | 2.39 | PHE141 – phenyl ring of benzamide<br>PHE198 – phenyl ring of benzamide | 2.16 (C=O, acidic) |
| **VIb** | 997.2 | −28.82 | O of GLY140 – H of acidic OH | 2.45 | PHE141 – phenyl ring of benzamide | 2.15 (C=O, acidic) |
| **VIe** | 672.7 | −33.44 | None | None | PHE141 – phenyl ring of benzamide<br>PHE198 – phenyl ring of benzamide | 2.14 (C=O, acidic) |
| **VIIa** | 629.5 | −30.35 | O of GLY140 – H of acidic OH | 2.41 | PHE141 – phenyl ring of benzamide | 2.17 (C=O, acidic) |
| **VIIf** | 725.2 | −44.75 | O of GLY140 – N of amide | 2.26 | PHE141 – phenyl ring of benzamide<br>PHE198 – phenyl ring of benzamide | 2.27 (C=O, amide) |
| **VIIIa** | 548.1 | −14.5 | HE2 of HIS170 – O of amidic C=O | 2.1 | PHE141 – phenyl ring of phthalic acid<br>PHE198 – phenyl ring of phthalic acid<br>PHE200 – phenyl ring of benzamide | Not significant |
| **VIIIe** | 526.9 | −17.95 | None | None | PHE141 – phenyl ring of benzamide<br>PHE198 – phenyl ring of benzamide | Not significant |

class I HDACs, based on the validated docking study that was performed prior to synthesis in the present study (−19% inhibition against HDAC2, −73% inhibition against HDAC3, −53% inhibition against HDAC8). Compound **IIIf (*E*)** showed potential enzyme inhibitory activity at 50 μM concentration against different HDAC isoforms (27% inhibition against HDAC6, 25% inhibition against HDAC8, 20% inhibition against HDAC5 and 15% inhibition against HDAC2), while compound **VIIa** showed no significant inhibitory activity at 50 μM concentration.

The enzyme inhibitory assay results were in consistency with the fact that carboxylic acid derivatives are poor HDAC inhibitors showing potential HDAC inhibitory activity at high doses [31,32]. Results implicates a potent zinc binding group is crucial for HDAC inhibitory activity. This work provided some insights to the binding interactions of inhibitors with HDAC and could facilitate development of novel hydroxamate and/or benzamide HDAC inhibitors from the novel synthesized carboxylic acid derivatives in this study in an attempt to synthesize more potent histone deacetylase inhibitors with stronger chelating groups.

### 4.2. Molecular modeling studies

#### 4.2.1. Docking study

Molecular docking was performed using Accelrys Discovery studio 2.5 software using the Dock ligands (CDOCKER) protocol which is an implementation of the CDOCKER algorithm. CDOCKER is a grid-based molecular docking method that employs CHARMm-based molecular dynamics (MD) scheme to dock ligands into a receptor binding site. Random ligand conformations are generated using high-temperature MD. It allows you to run a refinement docking of any number of ligands with a single protein receptor. Various scoring functions were applied to the ligands including -CDOCKER_ENERGY (CHARMm energy: interaction energy plus ligand strain) and -CDOCKER_INTERACTION_ENERGY: interaction energy only). Poses are sorted by CHARMm energy and the top scoring poses are calculated.

Molecular docking was based on crystal structures of HDLP (PDB ID: 1C3S) which is class I HDAC homologue complexed with SAHA (hydroxamic acid inhibitor of HDAC in crystal complex). Protein was prepared using prepare protein parameter which cleans

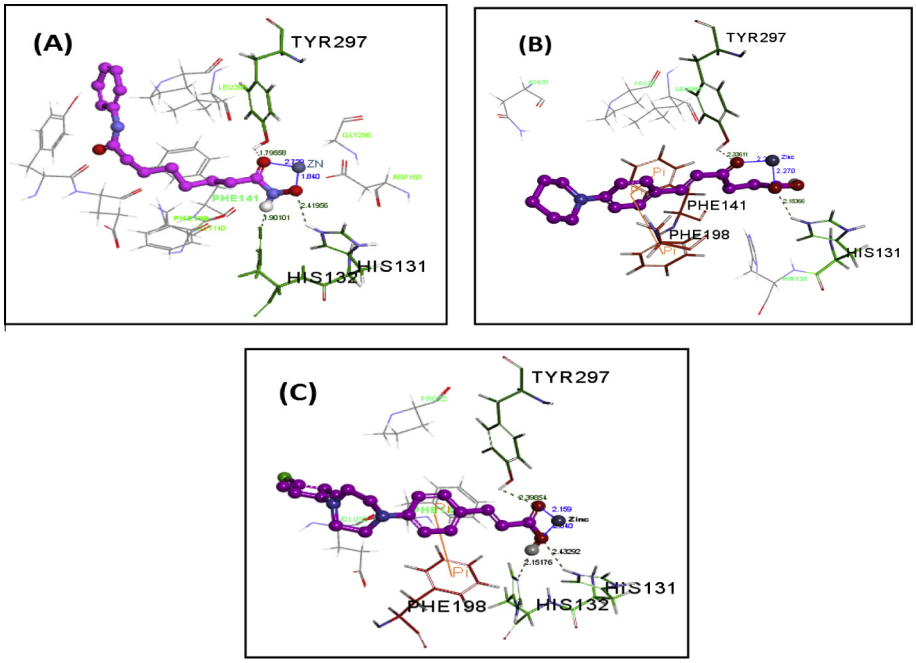


**Fig. 4.** Molecular modeling of original ligand (SAHA) and two newly synthesized compounds **IIc (*E*)** and **IIIg (*E*)** to compare binding interactions within the active site of HDLP (PDB ID: 1C3S). In (A) binding mode of original ligand (SAHA) with HDLP, (B) binding mode of newly synthesized compound **IIc (*E*)** with HDLP, (C) binding mode of newly synthesized compound **IIIg (*E*)** with HDLP. All interactions are described as H-bonds shown in dotted lines, pi–pi interactions shown in orange solid lines and metal coordination distance shown in blue lines. Amino acids involved in interactions and zinc metal were labelled.

up common problems in the input protein structure in preparation for further processing, where it inserts missing atoms in residues as hydrogen which was added and minimized and it also removes alternate conformations. All the waters were removed as well as all ions except for catalytic zinc ion. Synthesized compounds **IIb–f (*E*)**, **IIb**,**f (*Z*)**, **IIIa–g (*E*)**, **VIa**,**b**,**e**, **VIIa**,**f** and **VIIIa**,**e** were prepared from ligands prepare tool which adds hydrogen, fix bad valencies and generates a 3D coordinates using catalyst. Docking was performed using (CDOCKER) protocol. Pose cluster radius was set to 0.5 Å, top hits were set to 10 and other docking parameters were kept at default. Results were analyzed according to -CDOCKER_ENERGY.

*4.2.1.1. Docking results.* The binding modes of the synthesized carboxylic acids into the active site of histone deacetylase like protein (PDB ID: 1C3S) were in consistency with the proposed design and rational as described in Table 5. CDOCKER energy scores indicated favorable binding modes of SAHA and the newly synthesized compounds **IIc (*E*)** and **IIIg (*E*)** into the active site of HDLP (PDB ID: 1C3S) as shown in Fig. 4.

In (A), it was found that the CDOCKER energy score of the original ligand SAHA was −46.07 forming three hydrogen bond interactions between oxygen of hydroxamic hydroxyl group and histidine (His131) with a distance of 2.41 Å, hydrogen of hydroxamic NH and histidine (His132) with a distance of 1.90 Å and oxygen of amidic carbonyl group and tyrosine (Tyr297) with a distance of 1.79 Å. The distance between oxygen atom of amidic carbonyl group and oxygen of hydroxyl group with zinc ion were 1.79 Å and 1.84 Å, respectively. This was found to retrieve the reported [23] binding mode of SAHA in the X-ray crystal structure of HDLP (PDB ID: 1C3S).

In (B), the newly synthesized compound **IIc (*E*)** showed the best binding affinity with CDOCKER energy score of −51.03 and the most potent cytotoxic activity against HepG2 Cancer cell line (in which histone deacetylase enzyme is overexpressed) with measured $IC_{50}$ of 2.27 μM. Binding mode was consistent with SAHA, since compound **IIc (*E*)** forms two hydrogen bond interactions between oxygen of ketonic carbonyl group and tyrosine (Tyr297) with a distance of 2.33 Å and oxygen of acidic carbonyl group and histidine (His131) with a distance of 2.18 Å. Phenyl ring of styrene shows additional two pi–pi interaction with the phenyl rings of phenylalanine (Phe141) and phenylalanine (Phe198). The distance between the oxygen atom of ketonic carbonyl group and oxygen atom of acidic carbonyl group with zinc ion were 2.24 and 2.22 Å, respectively.

In (C), the newly synthesized compound **IIIg (*E*)** from series **III** showed the best binding affinity with CDOCKER energy score of −40.02 and the most significant cytotoxic activity with measured $IC_{50}$ of 10.63 μM. Binding mode was consistent with SAHA forming three hydrogen bond interactions between oxygen of acidic carbonyl group and tyrosine (Tyr297) with a distance of 2.39 Å, oxygen of acidic hydroxyl group and histidine (His131) with a distance of 2.43 Å and hydrogen of acidic hydroxyl group and histidine (His132) with a distance of 2.15 Å. Phenyl ring of styrene shows additional pi–pi interaction with phenyl ring of phenylalanine (Phe198). The distance between oxygen atom of acidic carbonyl group and oxygen atom of acidic hydroxyl group with zinc ion were 2.15 and 2.64 Å, respectively.

*4.2.1.2. Docking validation.* Validation of docking algorithm was achieved by docking of the selected lead compound, SAHA in the active site of histone deacetylase enzyme homologue (PDB ID:1C3S), this was found to retrieve the reported [23] binding mode of SAHA in the X-ray crystal structure of histone deacetylase enzyme homologue PDB (1C3S) as shown in Fig. 4(A). Nevertheless, the root mean square difference (RMSD) between the top docking pose and original crystallographic geometry of SAHA was 0.88 Å. This successful validation provides sufficient confidence in drawing meaningful conclusions from the docking study.

*4.2.2. Pharmacophore modeling*

In this study, pharmacophore generation was performed using Discovery Studio 2.5 software. The 3D QSAR pharmacophore Gen-

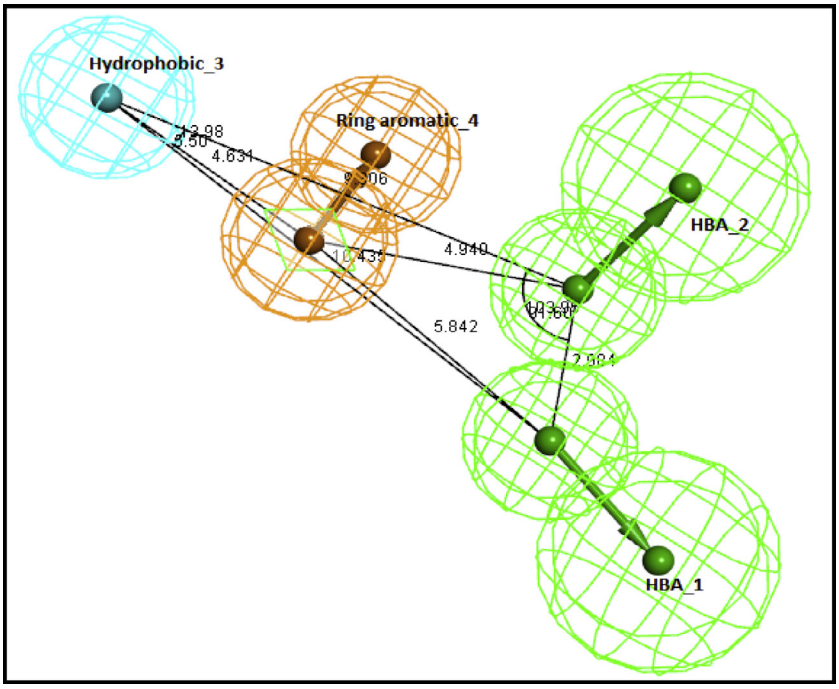


**Fig. 5.** Constraint distances and angles between features of the generated top pharmacophore model with the features considered hydrogen bond donor (HBA) colored in green, ring aromatic (RA) colored in orange, hydrophobic (HYP) colored in cyan.

**Table 6**
Constraint distances and angles between features of the generated top pharmacophore model.

| Constraint distances (Å) | Constraint angles (°) |
|---|---|
| (HBA_1) – (HBA_2), 2.984;<br>(HBA_1) – (RA_4), 5.842;<br>(HBA_2) – (RA_4), 4.940;<br>(HYP_3) – (HBA_1), 10.435;<br>(HYP_3) – (RA_4), 4.631;<br>(HYP_3) – (HBA_2), 9.306 | (HBA_1) – (HBA_2) – (HYP_3), 103.95;<br>(RA_4) – (HBA_2) – (HBA_1), 91.60;<br>(HBA_2) – (HYP_3) – (RA_4), 13.98;<br>(RA_4) – (HYP_3) – (HBA_1), 5.50 |

eration protocol (Catalyst HypoGen algorithm) was used to derive structure activity relationship hypothesis models (3D-QSAR pharmacophore models) from a set of ligands with known activity values on a given biological target [40].

The training set is composed of twenty-one synthesized compounds from the present study with measured $IC_{50}$ against HepG2 Cancer cell line for the generation of pharmacophore models considered as the certainty value. The uncertainty value was set as 1.5 instead of the default value 3.0. The pharmacophore features used are hydrogen bond acceptor (HBA), hydrogen bond donor (HBD), hydrophobic (HYP), ring aromatic (RA) and negative ionizable features. Though the Zn ion binding function is not included in the catalyst feature dictionary, it can be represented by the hydrogen bond acceptor or donor [40]. Fisher validation was applied and set to 95% significance. Pharmacophores were then generated in HypoGen module and the top nine scoring hypotheses were exported. HypoGen identifies features common to the active compounds and excludes features common to the inactive compounds within conformational allowable regions of space. It further estimates the activity of our newly synthesized and tested compounds using regression parameters. The parameters were computed by regression analysis using the relationship of geometric fit value versus the activity. The better the geometric fit the greater the activity prediction of the compound.

*4.2.2.1. Pharmacophore study results.* Nine predictive pharmacophore models (hypothesis) were generated via aligning different conformations of the represented training set ligands to bind with the generated pharmacophore models. These pharmacophore models were exported for further studies. All of the generated pharmacophore models contained at least four chemical features.

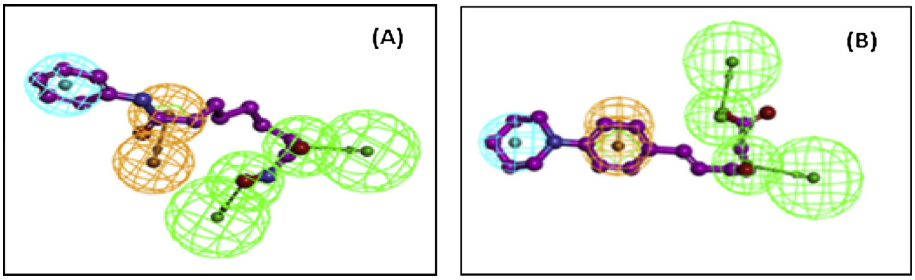


**Fig. 6.** The best generated pharmacophore model with the features considered hydrogen bond acceptor (HBA) colored in green, ring aromatic (RA) colored in orange, hydrophobic (HYP) colored in cyan where (A) shows SAHA fitted in the pharmacophore with fit value 5.90 (B) shows synthesized structure compound **IIc (*E*)** fitted in the pharmacophore with fit value 7.59.

**Table 7**
The pharmacophore features (hydrogen bond acceptor HBA_1, hydrogen bond acceptor HBA_2, hydrophobic feature HYP_3, and ring aromatic feature (RA)) mapped with the synthesized compounds and SAHA, as well as their fit values.

| Compd. | Fit value | HBA_1 | HBA_2 | HYP_3 | RA_4 |
|---|---|---|---|---|---|
| **IIb (*E*)** | 6.09 | CO of ketone | OH of carboxylic acid | Pyrrolidine | Phenyl ring of styrene |
| **IIb (*Z*)** | 5.29 | CO of ketone | – | Pyrrolidine | Phenyl ring of styrene |
| **IIc (*E*)** | 7.59 | CO of ketone | OH of carboxylic acid | Piperidine | Phenyl ring of styrene |
| **IId (*E*)** | 5.67 | – | CO of carboxylic acid | Morpholine | Phenyl ring of styrene |
| **IIe (*E*)** | 5.60 | – | OH of carboxylic acid | 4-$CH_3$-piperazine | Phenyl ring of styrene |
| **IIf (*E*)** | 6.76 | CO of ketone | OH of carboxylic acid | Piperazine | Phenyl ring of styrene |
| **IIf (*Z*)** | 5.03 | CO of ketone | – | Piperazine | Phenyl ring of styrene |
| **IIIa (*E*)** | 6.96 | CO of carboxylic acid | OH of carboxylic acid | Imidazole | Phenyl ring of styrene |
| **IIIb (*E*)** | 6.67 | CO of carboxylic acid | OH of carboxylic acid | Pyrrolidine | Phenyl ring of styrene |
| **IIIc (*E*)** | 6.67 | CO of carboxylic acid | OH of carboxylic acid | Piperidine | Phenyl ring of styrene |
| **IIId (*E*)** | 6.63 | CO of carboxylic acid | OH of carboxylic acid | Morpholine | Phenyl ring of styrene |
| **IIIe (*E*)** | 5.45 | OH of carboxylic acid | – | 4-$CH_3$-piperazine | Phenyl ring of styrene |
| **IIIf (*E*)** | 6.45 | CO of carboxylic acid | OH of carboxylic acid | Piperazine | Phenyl ring of styrene |
| **IIIg (*E*)** | 6.61 | CO of carboxylic acid | OH of carboxylic acid | Piperazine | Phenyl ring of styrene |
| **VIa** | 5.26 | OH of carboxylic acid | CO of amide | –––––––––– | Phenyl ring of benzamide |
| **VIb** | 5.04 | – | OH of carboxylic acid | Pyrrolidine | Phenyl ring of benzamide |
| **VIe** | 5.14 | CO of amide | – | 4-$CH_3$-piperazine | Phenyl ring of benzamide |
| **VIIa** | 5.13 | – | CO of amide | Imidazole | Phenyl ring of benzamide |
| **VIIf** | 5.09 | – | CO of carboxylic acid | Piperazine | Phenyl ring of benzamide |
| **VIIIa** | 5.19 | OH of carboxylic acid | CO of amide | – | Phenyl ring of benzamide |
| **VIIIe** | 5.21 | – | OH of carboxylic acid | Piperazine | Phenyl ring of benzamide |
| SAHA | 5.90 | CO of hydroxamic acid | OH of hydroxamic acid | Phenyl ring | – |

**Table 8**
Fit values and predicted activities for the synthesized compounds mapped with the generated 3D-pharmacophore model. SAHA mapping on the generated pharmacophore was used for further validation of the model.

| Compound | Predicted activity ($IC_{50}$ μM) | Experimental activity ($IC_{50}$ μM) | Fit value |
|---|---|---|---|
| **IIb (*E*)** | 68.08 | 63.58 | 6.09 |
| **IIb (*Z*)** | 437.1 | 413.9 | 5.29 |
| **IIc (*E*)** | 2.18 | 2.27 | 7.59 |
| **IId (*E*)** | 180.1 | 138.1 | 5.67 |
| **IIe (*E*)** | 212.1 | 904.8 | 5.60 |
| **IIf (*E*)** | 14.73 | 10.21 | 6.76 |
| **IIf (*Z*)** | 785.7 | 849.2 | 5.03 |
| **IIIa (*E*)** | 9.364 | 21.02 | 6.96 |
| **IIIb (*E*)** | 17.88 | 10.71 | 6.68 |
| **IIIc (*E*)** | 18.05 | 18.04 | 6.67 |
| **IIId (*E*)** | 19.81 | 45.69 | 6.63 |
| **IIIe (*E*)** | 302.2 | 430.7 | 5.45 |
| **IIIf (*E*)** | 32.14 | 32.85 | 6.42 |
| **IIIg** | 20.79 | 10.63 | 6.61 |
| **VIa** | 468.3 | 468.2 | 5.26 |
| **VIb** | 763.7 | 997.2 | 5.04 |
| **VIe** | 611.3 | 672.7 | 5.14 |
| **VIIa** | 627.8 | 629.5 | 5.13 |
| **VIIf** | 685.1 | 725.2 | 5.09 |
| **VIIIa** | 549.2 | 548.1 | 5.19 |
| **VIIIe** | 526.9 | 525.7 | 5.21 |
| SAHA | 72.26 | 63.48 [39] | 5.90 |

Five out of nine pharmacophore models had two HBA, one HYP, and one RA feature.

The top pharmacophore model generated, Hypothesis 5, was developed having two HBA, one HYP, and one RA feature as shown in Fig. 5 with constraint distances and angles between its features as described in Table 6.

In Fig. 6, SAHA and newly synthesized compound **IIc (*E*)** are represented with the best generated pharmacophore model. Where In (A) SAHA has fit value of 5.90 and its measured $IC_{50}$ is 63.48 μM [39] against HepG2 Cancer cell line. Three features out of four were considered, where carbonyl group of hydroxamic acids fits with (HBA_1), hydroxyl group of hydroxamic acid fits with (HBA_2) and phenyl ring fits with (HYP). While in (B) compound **IIc (*E*)** has highest fit value of 7.59 and highest cytotoxic activity against Human Liver HepG2 Cancer cell line with $IC_{50}$ of 2.27 μM. Four pharmacophore features were considered, where oxygen of ketonic carbonyl group fits with (HBA_1), oxygen of hydroxyl group fits with (HBA_2), pyridine ring fits with (HYP) and additionally the phenyl ring of styrene fits with (RA).

Features of the generated pharmacophore model mapped with the 21 synthesized compounds as well as SAHA are summarized in Table 7.

*4.2.2.2. Pharmacophore validation.* The pharmacophore models generated should be statistically significant, able to predict the activities of new chemical compounds and retrieve active compounds from the database. The selection of the generated pharmacophore model (Hypothesis 5) was be based on its validation using four methods; cost analysis, activity prediction, mapping of SAHA as a reported external reference to the generated pharmacophore and Fisher validation test.

HypoGen selects the best hypothesis by applying a cost analysis. The overall cost of each hypothesis is calculated by summing three cost factors, a weight cost, an error cost, and a configuration cost. However, configuration cost is the main contributor. HypoGen also calculates two theoretical costs, the null and fixed costs that can be used to determine the significance of the selected hypothesis. The fixed cost is the lowest possible cost representing a simplest hypothetical model that fits all data perfectly and the null cost represents the maximum cost of a pharmacophore with no features and estimates the activity to be the average activity of the training set compounds and the total cost for every pharmacophore. A larger difference between the fixed and null costs than that between the fixed and total costs of each hypothesis signifies the quality of a pharmacophore model. The significance of the hypothesis also depends on the cost difference which is measured between the null cost and the total cost of a given hypothesis. The larger the value of the cost difference, the more statistically significant the hypothesis is believed to be.

The quality of the generated pharmacophore hypothesis (Hypothesis 5) was evaluated by considering the cost functions calculation by HypoGen module during hypothesis generation. In detail, the null cost and fixed cost of the nine pharmacophore hypothesis were equal to 278.4 and 61.2, respectively. Hypothesis 5 is the best generated pharmacophore hypothesis as it is

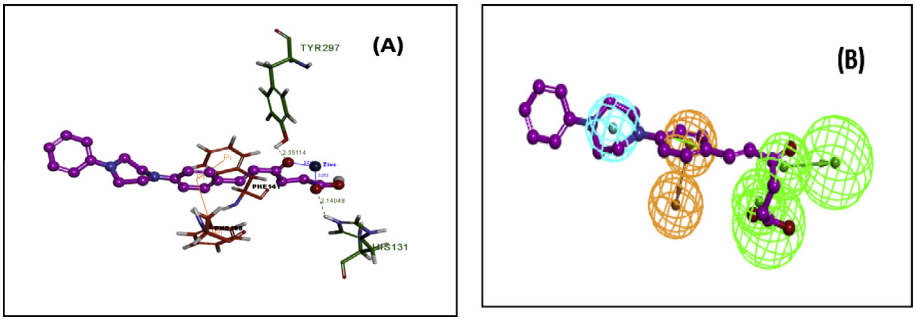


**Fig. 7.** Docking model (A) coincides with 3D QSAR pharmacophore model (B) for *E*-isomer of newly synthesized compound **IIf (*E*)** having a measured $IC_{50}$ against HepG2 Cancer cell line of 10.21 μM. In (A) compound **IIf (*E*)** was docked in the active site of HDAC (PDB code:1C3S) with a CDOCKER energy score of −48.71, interactions are described as H-bonds shown in dotted lines, pi–pi interactions shown in orange solid lines and metal coordination shown in blue lines, amino acids involved in interactions and zinc metal were labelled. In (B) compound **IIf (*E*)** fitted in the pharmacophore model with fit value 6.76. Features considered are hydrogen bond acceptor (HBA) colored in green, ring aromatic (RA) colored in orange and hydrophobic (HYP) colored in cyan.

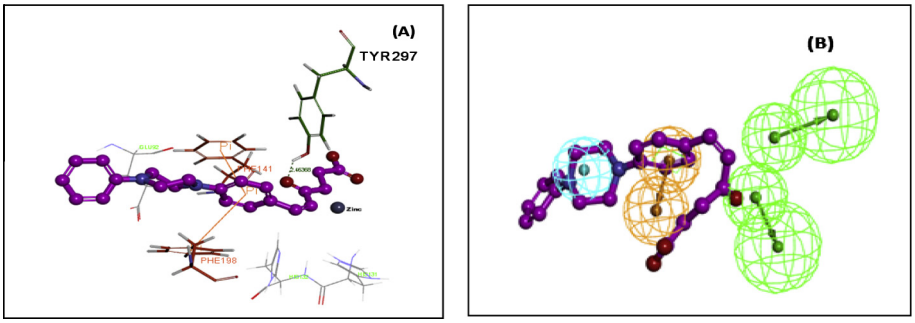


**Fig. 8.** Docking model (A) coincides with 3D QSAR pharmacophore model (B) for *Z*-isomer of newly synthesized compound **IIf (*Z*)** having a measured $IC_{50}$ of 849.2 μM. In (A) compound **IIf (*Z*)** was docked in the active site of HDAC (PDB code:1C3S) with a CDOCKER energy score of −28.4, interactions are described as H-bonds shown in dotted lines, pi–pi interactions shown in orange solid lines, amino acids involved in interactions and zinc metal were labelled. In (B) compound **IIf (*Z*)** fitted in the pharmacophore model with fit value 5.03. Features considered hydrogen bond acceptor (HBA) colored in green, ring aromatic (RA) colored in orange, hydrophobic (HYP) colored in cyan.

characterized by the lowest total cost (105.7), the highest cost difference between null and total hypothesis cost (172.7), and the best correlation coefficient (0.88) which indicates the capability of the pharmacophore model to predict the activity of the training set compounds.

The pharmacophore model (Hypothesis 5) was also validated through activity prediction of the synthesized structures as training set. Further validation for the pharmacophore model (Hypothesis 5) generated was performed through mapping of SAHA using ligand pharmacophore mapping protocol, comparing its fit value with the fit values of the tested compounds which was detected as 5.90 and comparing its predicted activity with its experimental activity. The predicted activities of SAHA and the training set through the pharmacophore model as well as their fit values are represented in Table 8. It should be noted that the predicated anti-proliferative activities by the 3D pharmacophore QSAR model were very close to those experimentally observed, indicating that these models can be safely applied for prediction of cytotoxic activity of newly synthesized compounds.

Fischer validation is another approach for pharmacophore model validation. The Fischer validation confidence level for Hypothesis 5 is 95%. This validation method checks the correlation between the chemical structures and biological activity. This method generates pharmacophore hypothesis using the same parameters as those used to develop the original pharmacophore hypothesis by randomizing the activity data of the training set compounds.

*4.2.2.3. Conclusion.* In conclusion, results of cytotoxic activity against Liver HepG2 Cancer cell line were consistent with pharmacophore fit score values and docking score energies. Where it was observed that compound **IIc (*E*)** ((*E*)-6-(4-(piperidin-1-yl)phenyl)-4-oxo-hex-5-enoic acid) with the lowest $IC_{50}$ of 2.27 μM (i.e. most potent), showed the best fit value of 7.59 and the highest binding affinity with CDOCKER energy score of −50.27.

Interestingly, 3D QSAR pharmacophore model created to explore the observed cytotoxic activity against HepG2 Cancer cell line for the *E* and *Z* isomers of the newly synthesized compound **IIf** coincides with docking. This enabled an explanation for the increase of cytotoxic activity of compound **IIf (*E*)** having an $IC_{50}$ of 10.21 μM when compared with its *Z* isomer **IIf (*Z*)** having an $IC_{50}$ of 849.2 μM.

In Fig. 7, compound **IIf (*E*)** has CDOCKER energy score of −48.71, where its two oxygen atoms of ketonic and acidic carbonyl accepts two hydrogen atoms from tyrosine (Tyr297) and histidine (His131) respectively. And its phenyl ring of styrene forms two pi–pi interaction with phenylalanine (Phe141) and phenylalanine (Phe198). The respective distance between the oxygen atoms of ketonic and acidic carbonyl with zinc ion were 2.21 and 2.27 Å, which enabled the coordination of zinc ion. Also compound **IIf (*E*)** has fit value of 6.76 fitting with the four features of the generated pharmacophore model. Where oxygen of ketonic carbonyl group fits with (HBA_1), oxygen of acidic carbonyl fits with (HBA_2), piperazine fits with (HYP_3) and phenyl ring of styrene fits with RA_4.

While compound **IIf (*Z*)** has CDOCKER energy score of −28.4 score, where oxygen of ketonic carbonyl accepts one hydrogen atom from tyrosine (Tyr297) and its phenyl ring of styrene forms two pi–pi interaction with Phe141 and Phe198. The measured distance of its ketonic carbonyl with zinc ion was 7.44 Å, which showed inability to coordinate the zinc ion. Also, compound **IIf (*Z*)** has the lowest fit value of 5.03 and fits with only three features of the pharmacophore model generated. Where oxygen of ketonic carbonyl group fits with (HBA_1), piperazine fits with (HYP_3) and phenyl ring of styrene fits with (RA_4) as shown in Fig. 8.

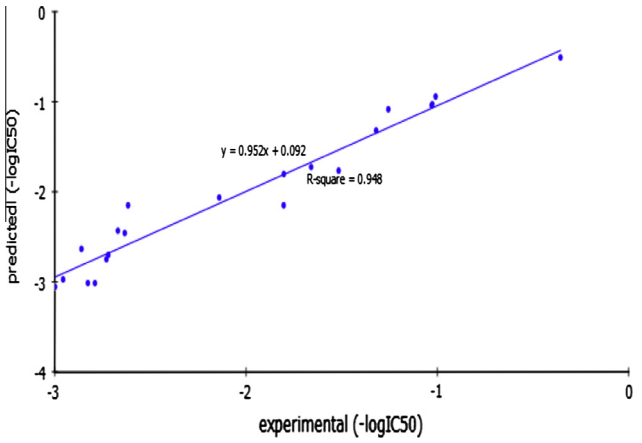


**Fig. 9.** Shows the corresponding scatter plots of the experimental versus the predicted bioactivity values $-\log IC_{50}$ for the training set compounds according to Eq. (1). ($r^2 = 0.948$).

**Table 9**
Experimental activity of the synthesized compounds against the predicted activity according to Eq. (1).

| Compd. | Experimental activity ($-\log IC_{50}$) | Predicted activity ($-\log IC_{50}$) | Residual |
|---|---|---|---|
| **IIb (*E*)** | −1.803 | −2.149 | 0.346 |
| **IIb (*Z*)** | −2.616 | −2.149 | −0.467 |
| **IIc (*E*)** | −0.356 | −0.508 | 0.152 |
| **IId (*E*)** | −2.140 | −2.063 | −0.076 |
| **IIe (*E*)** | −2.956 | −2.973 | 0.016 |
| **IIf (*E*)** | −1.009 | −0.942 | −0.066 |
| **IIIa (*E*)** | −1.32 | −1.32 | 0.000 |
| **IIIb (*E*)** | −1.029 | −1.041 | 0.011 |
| **IIIc (*E*)** | −1.256 | −1.083 | −0.172 |
| **IIId (*E*)** | −1.659 | −1.725 | 0.065 |
| **IIIe (*E*)** | −2.634 | −2.458 | −0.175 |
| **IIIf (*E*)** | −1.516 | −1.765 | 0.249 |
| **IIIg (*E*)** | −1.026 | −1.026 | 0.000 |
| **VIa** | −2.67 | −2.432 | −0.237 |
| **VIb** | −2.998 | −3.056 | 0.057 |
| **VIe** | −2.827 | −3.013 | 0.186 |
| **VIIa** | −2.79 | −3.014 | 0.224 |
| **VIIf** | −2.860 | −2.634 | −0.226 |
| **VIIIa** | −2.730 | −2.748 | 0.018 |
| **VIIIe** | −2.720 | −2.701 | −0.018 |

From series **III**, compound **IIIg (*E*)** ((*E*)-3-(4-(4-(4-chlorophenyl)piperazin-1-yl)phenyl)acrylic acid) with the lowest measured $IC_{50}$ of 10.63 μM, has the best fit value of 6.61 and highest binding affinity with CDOCKER energy score of −40.02.

While all synthesized compounds of series **VI** (4-(4-(substituted)phenylamino)-4-oxobutanoic acid), **VII** (5-(4-(substituted)phenylamino)-5-oxopentanoic acid) and **VIII** (2-((4-substituted)phenyl) carbamoyl) benzoic acid) have insignificant cytotoxic activity $IC_{50} > 100$ μM, lowest binding affinity and lowest fit value ranging from 5.04 to 5.26.

*4.2.3. 2D QSAR study*

The QSAR study was performed using Discovery Studio 2.5 Software. The training set was composed of the twenty-one synthesized compounds from the present study with their measured $pIC_{50}$ ($-\log IC_{50}$) against HepG2 Cancer cell line for QSAR modeling. "Calculate Molecular Properties" module was used for calculating the 2D and 3D molecular properties as well as energies of highest occupied and lowest unoccupied molecular orbitals (HOMO and LUMO) [41] of the training set compounds.

2D Descriptors involved: AlogP, fingerprints, molecular properties, surface area and volume, as well as topological descriptors, and the 3D descriptors: dipole, Jurs descriptors, principle moments of inertia, and shadow indices.

Furthermore, the training set compounds were fitted against representative pharmacophores and their fit values were added as additional descriptors. The fit values of the training set compounds were calculated automatically using the previously described "3D QSAR Pharmacophore Generation" module.

Multiple linear regression (MLR) analysis was employed to search for optimal QSAR models that combine high quality binding pharmacophores with other molecular descriptors and being capable of correlating bioactivity variation across the used training set collection. Compound **IIf (*Z*)** was identified as a statistical outlier. QSAR model was validated employing leave one-out cross-validation by setting the folds to a number much larger than the number of samples, $r^2$ (squared correlation coefficient value) and $r^2$ prediction (predictive squared correlation coefficient value), residuals between the predicted and experimental activity of the test set and training set [42].

*4.2.3.1. QSAR study results.* Eq. (1) represents the best performing QSAR model.

$$-\log IC_{50} = -1260.8\,A\log P - 4.059\,pKa[1] - 3.313\,pKa[2] - 109.98 \times \text{Molecular\_Fractional Polar Surface Area} + 2042.3 \quad (1)$$

*Abbreviations used*: $-\log IC_{50}$ is the negative logarithmic value of the concentration required to produce 50% inhibition of HepG2 Cancer cells. AlogP is a measure of the hydrophobicity of the molecule; it is calculated in Discovery Studio as the log of the octanol–water partition coefficient using Ghose and Crippen's method [43]; p*K*a is the p*K*a value of all ionizable sites; Molecular_Fractional Polar Surface Area is the ratio of the polar surface area divided by the total surface area of the molecule.

According to Eq. (1) QSAR model is represented graphically by scattering plots of the experimental versus the predicted bioactivity values $-\log IC_{50}$ for the training set compounds as shown in Fig. 9.

The method used to build the model was Least-Squares, $r^2 = 0.948$, $r^2$ (adj) 1.017, $r^2$ (pred) 0.215, Least-squared error 0.033155, where **$r^2$ (adj)** is $r^2$ adjusted for the number of terms in the model; **$r^2$ (pred)** is the prediction $r^2$, equivalent to $q^2$ from a leave-1-out cross-validation.

Knowledge of p*K*a values together with partition coefficient can be used for estimating the extent to which the compound enters the bloodstream. Enzyme kinetics are dependent on the p*K*a values of many acids and bases and is also a prerequisite for a quantitative understanding of the interaction between acids and bases and metal ions to form complex. In conclusion, Eq. (1) describes that the cytotoxic activity of synthesized compounds on Liver HepG2 Cancer cell line is affected by three molecular descriptors AlogP, p*K*a and molecular fractional polar surface, where cytotoxic activity is increased by decreasing the hydrophobicity (AlogP), p*K*a value of all ionizable sites and decreasing the molecular fractional polar surface area of the synthesized compounds.

*4.2.3.2. QSAR validation.* QSAR models were validated internally employing leave-1-out cross-validation where $r^2$ (squared correlation coefficient value) which is 0.948, **$r^2$ (pred)** is the prediction $r^2$, equivalent to $q^2$ from a leave-1-out cross-validation which is 0.215. Validation was also employed by measuring the residuals between the experimental activity and the predicted activity of the training set. The experimental activities and those predicted by QSAR studies were presented in Table 9. It should be noted that the predicated anti-proliferative activities by our QSAR models were very close to those experimentally observed, indicating that these

models can be safely applied for prediction of more effective hits having the same skeletal framework.

## 5. Conclusion

In summary, it was found that docking coincides with 3D QSAR pharmacophore model generated for the displayed cytotoxic activity of the synthesized compounds against HepG2 Cancer cell line.

It was revealed that *E*-isomers for compounds **IIb**, **IIf** displayed significant cytotoxic activity compared to their *Z*-isomers which showed insignificant cytotoxic activity. Compounds **IIc (*E*)**, **IIf (*E*)**, **IIIb (*E*)**, and **IIIg (*E*)** displayed the highest cytotoxic activity against HepG2 human cancer cell lines with $IC_{50}$ ranging from 2.27 to 10.71 μM. Compound **IIf (*E*)** ($NHR_2$ = phenylpiperazine) displayed significant cytotoxic activity against NCI Non-Small Cell Lung A549/ATCC Cancer cell line (68% inhibition activity), NCI-H460 Cancer cell line (66% inhibition activity) and Liver HepG2 Cancer cell line ($IC_{50}$, 10.21 μM). And unpredictably, compound **IIf (*E*)** showed remarkable stimulation of HDAC activity toward different HDAC isoforms instead of the expected inhibitory activity against class I HDACs. It is suggested that the significant cytotoxic effect of compound **IIf (*E*)** is maybe due to another mechanism of action. Compound **IIIf (*E*)** ($NHR_2$ = phenylpiperazine) showed significant inhibitory activity (57.34%) against NCI Breast MDA-MB-468 Cancer cell line and potential HDAC inhibitory activity against different HDAC isoforms (20% HDAC5, 27% HDAC6 and 25% HDAC8).

It was found that the major structural factors affecting the potency of these compounds were related to their basic skeleton. The results indicated that the carboxylic acid derivatives of series **II** and **III** could serve as promising lead compounds for further optimization.

## 6. Experimental protocols

### 6.1. Chemistry

Starting materials and reagents were purchased from Sigma–Aldrich and Merck and used without further purification. Melting points were recorded on Stuart Scientific apparatus and were uncorrected. Reactions were monitored using thin layer chromatography (TLC), performed on 0.255 mm silica gel plates, with visualization under U.V. light (254 nm). FT-IR spectra were recorded on a 4100 Jasco spectrophotometer using KBr disk in the Microanalytical center, Cairo University. 1H NMR spectra were recorded in δ scale given in ppm on Varian Mercury VX-300 NMR spectrometer in NMR Lab, Chemistry Department, Faculty of Science, Cairo University and Varian Mercury VX-400 NMR spectrometer in NMR Lab, Chemistry Department, Faculty of Pharmacy, Cairo University. Coupling patterns are described as follows: s, singlet; d, doublet; t, triplet; m, multiplet; and 1H, 2H, 3H, etc. *J* describes a coupling constant. The coupling constants were rounded off to one decimal place. MS spectra mass were recorded on Shimadzu GCMS-QP 1000 EX gas chromatograph mass spectrometer in the Microanalytical center, Cairo University. Elemental analyses were performed at the Microanalytical Center, Azhar University.

#### 6.1.1. General method for preparation of 4-(substituted) benzaldehyde (***Ia–g***) [34]

A mixture of p-fluorobenzaldehyde **1** (25.0 g, 0.200 mol) and appropriate amine **2a–g** (0.300 mol) and anhydrous potassium carbonate (40.0 g) were mixed in DMF (300 mL), after which catalytic amount of Aliquat 336 reagent was added. The mixture was then refluxed for 24 h at 100 °C. The mixture was concentrated under low pressure and left to cool. The mixture was then poured into ice water and left overnight. The formed solid was filtered, washed with water and crystallized with methanol to yield compounds **Ia–g**.

*6.1.1.1. 4-(1H-imidazol-1-yl) benzaldehyde **Ia**.* Yield 92% as yellow crystals, mp 152 °C, (as reported) [34,44].

*6.1.1.2. 4-(Pyrrolidin-1-yl) benzaldehyde **Ib**.* Yield 98% as yellow crystals, mp 85 °C, (as reported) [45,46].

*6.1.1.3. 4-(Piperidin-1-yl) benzaldehyde **Ic**.* Yield 98% as yellow crystals, mp 64 °C, (as reported) [47,48].

*6.1.1.4. 4-Morpholinobenzaldehyde **Id**.* Yield 89% as yellow crystals, mp 69 °C, (as reported) [49,50].

*6.1.1.5. 4-(4-Methylpiperazin-1-yl) benzaldehyde **Ie**.* Yield 87% as yellow crystals, mp 64 °C, (as reported) [45,51].

*6.1.1.6. 4-(4-Phenylpiperazin-1-yl) benzaldehyde **If**.* Yield 98% as yellow crystals, mp 134 °C, (as reported) [52].

*6.1.1.7. 4-(4-(4-Chlorophenyl) piperazin-1-yl) benzaldehyde **Ig**.* Yield 92% as yellow crystals, mp 133 °C. IR: (Ú max, $cm^{-1}$): 1685 (C=O, CHO), 2724–2822 (C<u>H</u>O). $^1$H NMR (300 MHz)($CDCl_3$) δ: 3.26 (t, 4H, piperazine $H_3$, $H_5$, *J* = 5.1 Hz), 3.56 (t, 4H, piperazine $H_2$, $H_6$, *J* = 5.1 Hz), 6.91–7.04 (m, 6H, aromatic Hs), 7.79 (d, 2H, aromatic $H_{3'}$, $H_{5'}$, *J* = 9 Hz), 9.82 (s, 1H, C<u>H</u>O). MS: *m/z* (%): 300 ($M^+$, 89%) and base peak at 105 (100%).

#### 6.1.2. General method for preparation of (E)-6-(4-(substituted) phenyl)-4-oxohex-5-enoic acid ***IIb–f*** and (Z)-6-(4-(substituted) phenyl)-4-oxohex-5-enoic acid ***IIb,f*** [35]

A mixture of the respective aldehyde **Ib–f** (0.003 mol) and levulinic acid (0.003 mol) were dissolved in benzene (100 mL) containing acetic acid (3 mL) and piperidine (1 mL). The solution was heated under reflux using Dean–Stark water trap under nitrogen until the theoretical amount of water had been collected (~6 h). The solvent was then evaporated under vacuum and the formed solid product was washed twice with 10 mL of diethyl ether and then twice with 15 mL of 2 M HCl. The product was dried and purified using solvent crystallization or column chromatography (as illustrated below).

*6.1.2.1. (E)-6-(4-(pyrrolidin-1-yl)phenyl)-4-oxo-hex-5-enoic acid **IIb (E)**.* Purified by silica gel column chromatography using hexane/ethyl acetate 8:2 eluent with *E*/*Z* ratio 1–3 respectively. Yield 25% as red solid, mp 155 °C. IR: (Ú max, $cm^{-1}$): 1600 (C=C), 1651 (C=O, ketonic), 1712 (C=O, COOH), 2949–3429 (OH, COOH). $^1$H NMR (300 MHz)($CDCl_3$) δ: 2.04 (t, 4H, pyrrolidine $H_3$, $H_4$, *J* = 6.6 Hz), 2.73 (t, 2H, $CH_2$—C<u>H</u>$_2$—COOH, *J* = 6.6 Hz), 3.03 (t, 2H, C<u>H</u>$_2$—$CH_2$—COOH, *J* = 6.6 Hz), 3.40 (t, 4H, pyrrolidine $H_2$, $H_6$, *J* = 6.6 Hz), 6.61 (d, 1H, CH=C<u>H</u>—CO, *J* = 16.2 Hz), 6.61 (d, 2H, aromatic $H_2$, $H_6$, *J* = 8.4 Hz), 7.45 (d, 2H, aromatic $H_3$, $H_5$, *J* = 8.4 Hz), 7.61 (d, 1H, C<u>H</u>=CH—CO, *J* = 15.9 Hz). MS: *m/z* (%): 273 ($M^+$, 100%), 275 ($M^+$+2, 8%). Anal. Calcd for $C_{16}H_{19}NO_3$: C, 70.31; H, 7.01; N, 5.12. Found: C, 70.42; H, 7.13; N, 5.19.

*6.1.2.2. (Z)-6-(4-(pyrrolidin-1-yl)phenyl)-4-oxo-hex-5-enoic acid **IIb (Z)**.* Purified by silica gel column chromatography using hexane/ethyl acetate 8:2 eluent with *Z*/*E* ratio 3–1 respectively. Yield 75% as yellow solid, mp 188 °C. IR: (Ú max, $cm^{-1}$): 1600 (C=C), 1644 (C=O, ketonic), 1709 (C=O, COOH), 2964–3445 (OH, COOH). $^1$H NMR (400 MHz)(DMSO) δ: 1.95 (t, 4H, pyrrolidine $H_3$, $H_4$, *J* = 6.4 Hz), 2.50 (t, 2H, $CH_2$—C<u>H</u>$_2$—COOH, *J* = 6.4 Hz), 2.88 (t, 2H, C<u>H</u>$_2$—$CH_2$—COOH, *J* = 6.4 Hz), 3.32 (t, 4H, pyrrolidine $H_2$, $H_6$, *J* = 6.4 Hz), 6.58 (d, 1H, CH=C<u>H</u>—CO, *J* = 8.8 Hz), 6.59–6.63 (m, 2H, aromatic $H_2$, $H_6$), 7.50 (m, 2H, aromatic $H_3$, $H_5$), 7.54 (d, 1H, C<u>H</u>=CH—CO, *J* = 8.8 Hz), 12.05 ($s_{br}$, 1H, COO<u>H</u>). MS: *m/z* (%): 273 ($M^+$, 40%), 274 ($M^+$+1, 28%) and base peak at 64 (100%). Anal. Calcd

for $C_{16}H_{19}NO_3$: C, 70.31; H, 7.01; N, 5.12. Found: C, 70.42; H, 7.13; N, 5.19.

*6.1.2.3. (E)-6-(4-(piperidin-1-yl)phenyl)-4-oxo-hex-5-enoic acid* ***IIc (E)***. Yield 60% as reddish purple crystals (recrystallized from ethanol), mp 176 °C. IR: (Ú max, $cm^{-1}$): 1600 (C=C), 1627 (C=O, ketonic), 1751 (C=O, COOH), 2928–3440 (OH, COOH). $^1$H NMR (300 MHz)($CDCl_3$) δ: 1.69 ($s_{br}$, 8H, piperidine $H_3$, $H_4$, $H_5$ and $CH_2$—C$\underline{H_2}$—COOH), 3.37 ($s_{br}$, 6H, piperidine $H_2$, $H_6$ and C$\underline{H_2}$—$CH_2$—COOH), 6.61 (d, 1H, CH=C$\underline{H}$—CO, *J* = 16.2 Hz), 6.89 (d, 2H, aromatic $H_2$, $H_6$, *J* = 8 Hz), 7.17 (d, 1H, C$\underline{H}$=CH—CO, *J* = 16.2 Hz), 7.51–7.54 (d, 2H, aromatic $H_3$, $H_5$, *J* = 8 Hz). MS: *m/z* (%): 287 ($M^+$, 17.8%), 288 ($M^+$+1, 5.5%) and base peak at 213 (100%). Anal. Calcd for $C_{17}H_{21}NO_3$: C, 71.06; H, 7.37; N, 4.87. Found: C, 71.22; H, 7.43; N, 4.93.

*6.1.2.4. (E)-6-(4-morpholinophenyl)-4-oxo-hex-5-enoic acid* ***IId (E)***. Yield 56% as yellow crystals (recrystallized from ether/petroleum ether), mp 101 °C. IR: (Ú max, $cm^{-1}$): 1507 (C=C), 1644 (C=O, ketonic), 2964–3440 (OH, COOH). $^1$H NMR (300 MHz)($CDCl_3$) δ: 2.69 (t, 2H, $CH_2$—C$\underline{H_2}$—COOH, *J* = 6.6 Hz), 3.08 (t, 2H, C$\underline{H_2}$—$CH_2$—COOH, *J* = 6.6 Hz), 3.58–3.70 (m, 8H, morpholine H), 6.75 (d, 1H, CH=C$\underline{H}$—CO, *J* = 15.9 Hz), 7.08 (d, 2H, aromatic $H_2$, $H_6$, *J* = 8.7 Hz), 7.55 (d, 2H, aromatic $H_3$, $H_5$, *J* = 8.7 Hz), 7.60 (d, 1H, C$\underline{H}$=CH—CO, *J* = 15.9 Hz). MS: *m/z* (%): 287 ($M^+$–2, 1.58%) and base peak at 149 (100%). Anal. Calcd for $C_{16}H_{19}NO_4$: C, 66.42; H, 6.62; N, 4.84. Found: C, 66.61; H, 6.70; N, 4.89.

*6.1.2.5. (E)-6-(4-(4-methylpiperazin-1-yl)phenyl)-4-oxo-hex-5-enoic acid* ***IIe (E)***. Yield 60% as yellow crystals (recrystallized from methanol), mp 190 °C. IR: (Ú max, $cm^{-1}$): 1590 (C=C), 1680 (C=O, ketonic), 2955–3423 (OH, COOH). $^1$H NMR (300 MHz)($CDCl_3$) δ: 2.44 (s, 3H, $CH_3$-piperazine), 2.58 (t, 2H, $CH_2$—C$\underline{H_2}$—COOH, *J* = 6.3 Hz), 2.73 (t, 4H, piperazine $H_3$, $H_5$, *J* = 5.1 Hz), 3.01 (t, 2H, C$\underline{H_2}$—$CH_2$—COOH, *J* = 6.3 Hz), 3.35 (t, 4H, piperazine $H_2$, $H_6$, *J* = 4.8 Hz), 6.64 (d, 1H, CH=C$\underline{H}$—CO, *J* = 16.2 Hz), 6.87 (d, 2H, aromatic $H_2$, $H_6$, *J* = 8 Hz), 7.43 (d, 2H, aromatic $H_3$, $H_5$, *J* = 8 Hz), 7.54 (d, 1H, C$\underline{H}$=CH—CO, *J* = 16.2 Hz). MS: *m/z* (%): 302 ($M^+$, 100%), 304 ($M^+$+2, 2.06%). Anal. Calcd for $C_{17}H_{22}N_2O_3$: C, 67.53; H, 7.33; N, 9.26. Found: C, 67.68; H, 7.41; N, 9.34.

*6.1.2.6. (E)-6-(4-(4-phenylpiperazin-1-yl)phenyl)-4-oxohex-5-enoic acid* ***IIf (E)***. Purified by silica gel column chromatography using hexane/ethyl acetate 8:2 eluent with *E*/*Z* ratio 1–2 respectively. Yield 35% as yellow needle crystals, mp 171 °C. IR: (Ú max, $cm^{-1}$): 1596 (C=C), 1693 (C=O, ketonic), 1701 (C=O, COOH), 2954–3429 (OH, COOH). $^1$H NMR (300 MHz)($CDCl_3$) δ: 2.68 (t, 2H, $CH_2$—C$\underline{H_2}$—COOH, *J* = 6.6 Hz), 3.02 (t, 2H, C$\underline{H_2}$—$CH_2$—COOH, *J* = 6.3 Hz), 3.25 (t, 4H, piperazine $H_3$, $H_5$, *J* = 5.4 Hz), 3.42 (t, 4H, piperazine $H_2$, $H_6$, *J* = 5.7 Hz), 6.66 (d, 1H, CH=C$\underline{H}$—CO, *J* = 16.2 Hz), 6.92 (d, 2H, aromatic $H_{2'}$, $H_{6'}$, *J* = 7.5 Hz), 6.95–7.00 (m, 2H, aromatic $H_3$, $H_5$), 7.27–7.28 (m, 1H, aromatic $H_{4'}$), 7.34 (d, 2H, aromatic $H_{3'}$, $H_{5'}$, *J* = 7.8 Hz) 7.50 (d, 2H, aromatic $H_2$, $H_6$, *J* = 6.6 Hz), 7.58 (d, 1H, C$\underline{H}$=CH—CO, *J* = 16.2 Hz). MS: *m/z* (%): 364 ($M^+$, 17%), 365 ($M^+$+1, 21.86%) and base peak at 105 (100%). Anal. Calcd for $C_{22}H_{24}N_2O_3$: C, 72.50; H, 6.64; N, 7.69. Found: C, 72.59; H, 6.69; N, 7.82.

*6.1.2.7. (Z)-6-(4-(4-phenylpiperazin-1-yl)phenyl)-4-oxohex-5-enoic acid* ***IIf (Z)***. Purified by silica gel column chromatography using hexane/ethyl acetate 8:2 eluent with *Z*/*E* ratio 2–1 respectively. Yield 62.5% as orange solid, mp 230 °C. IR: (Ú max, $cm^{-1}$): 1509 (C=C), 1592 (C=O, ketonic), 2966–3446 (OH, COOH). $^1$H NMR (300 MHz)($CDCl_3$) δ: 2.28 (t, 2H, $CH_2$—C$\underline{H_2}$—COOH), 2.99 (t, 2H, C$\underline{H_2}$—$CH_2$—COOH), 3.45 (s, 4H, piperazine $H_3$, $H_5$), 3.56 (s, 4H, piperazine $H_2$, $H_6$), 6.82 (d, 1H, CH=C$\underline{H}$—CO), 7.00–7.14 (m, 5H, phenyl piperazine aromatic H's), 7.25 (d, 1H, C$\underline{H}$=CH—CO, *J* = 6.4 Hz), 7.65 (d, 2H, aromatic $H_3$, $H_5$, *J* = 8.4 Hz), 7.76 (d, 2H, aromatic $H_2$, $H_6$, *J* = 8.2 Hz). MS: *m/z* (%): 364 ($M^+$, 3.81%) and base peak at 65 (100%). Anal. Calcd for $C_{22}H_{24}N_2O_3$: C, 72.50; H, 6.64; N, 7.69. Found: C, 72.59; H, 6.69; N, 7.82.

*6.1.3. General method for preparation of (E)-3-(4-substituted phenyl)acrylic acid* ***IIIa–g*** *[53]*

A mixture of 0.208 g. (0.002 mol) of malonic acid and 0.166 g. (0.001 mol) of 4-substituted benzaldehyde **Ia–g** and (5 mL) of pyridine was prepared. Malonic acid is dissolved by shaking and warming on a steam bath. Catalytic amount of piperidine was then added and the mixture was heated at 80–85 °C for 1 h. After which the mixture was heated under reflux (109–115 °C) for an additional 3 h. The reaction mixture was then cooled and poured into cold water. The mixture was then acidified by slow addition of concentrated hydrochloric acid with stirring. The formed light crystals were separated by filtration and washed 4 times with cold water. The crude acid was dissolved in a solution of 5% sodium hydroxide. The resulting solution was filtered, diluted with an additional water, and acidified by adding concentrated hydrochloric acid. The formed solid was filtered and washed with cold water. The solid was further purified by using methanol as the solvent of crystallization to yield titled compounds **IIIa–g**.

*6.1.3.1. (E)-3-(4-(1H-imidazol-1-yl)phenyl) acrylic acid* ***IIIa (E)***. Yield 75% as pale white solid, mp 326 °C, (as reported) [54,55].

*6.1.3.2. (E)-3-(4-(Pyrrolidin-1-yl)phenyl) acrylic acid* ***IIIb (E)***. Yield 85% as yellow solid, mp 265 °C, (as reported) [54,56].

*6.1.3.3. (E)-3-(4-(Piperidin-1-yl)phenyl) acrylic acid* ***IIIc (E)***. Yield 87% as reddish purple solid, mp 110 °C. IR: (Ú max, $cm^{-1}$): 1594 (C=C), 1755 (C=O, COOH), 2928–3420 (OH, COOH). $^1$H NMR (400 MHz)(DMSO) δ: 1.54 (m, H, piperidine $H_3$, $H_4$, $H_5$), 3.39 (t, 4H, piperidine $H_2$, $H_6$), 6.47 (d, 1H, CH=C$\underline{H}$—COOH, *J* = 16 Hz), 7.01 (d, 2H, aromatic $H_3$, $H_5$, *J* = 8.8 Hz), 7.50 (d, 1H, C$\underline{H}$=CH—COOH, *J* = 15.8 Hz), 7.65 (d, 2H, aromatic $H_2$, $H_6$, *J* = 8.8 Hz). MS: *m/z* (%): 231 ($M^+$, 77%), 232 ($M^+$+1, 58%) and base peak at 209 (100%). Anal. Calcd for $C_{14}H_{17}NO_2$: C, 72.70; H, 7.41; N, 6.06. Found: C, 72.84; H, 7.48; N, 6.19.

*6.1.3.4. (E)-3-(4-Morpholinophenyl) acrylic acid* ***IIId (E)***. Yield 75% as orange solid, mp 198 °C, (as reported) [57].

*6.1.3.5. (E)-3-(4-(4-Methyl piperazin-1-yl)phenyl) acrylic acid* ***IIIe (E)***. Yield 90% as yellow solid, mp 228 °C, (as reported) [54].

*6.1.3.6. (E)-3-(4-(4-Phenylpiperazin-1-yl)phenyl) acrylic acid* ***IIIf*** *(E).* Yield 90% as yellow solid, mp 240 °C. IR: (Ú max, $cm^{-1}$): 1600 (C=C), 1759 (C=O, COOH), 2920–3452 (OH, COOH). $^1$H NMR (400 MHz)(DMSO) δ: 3.24 (t, 4H, piperazine $H_3$, $H_5$, *J* = 4.8 Hz), 3.48 (t, 4H, piperazine $H_2$, $H_6$, *J* = 4.8 Hz), 6.25 (d, 1H, CH=C$\underline{H}$—COOH, *J* = 15.6 Hz), 6.74–7.21 (m, 5H, phenyl piperazine aromatic Hs), 7.46 (d, 1H, C$\underline{H}$=CH—COOH, *J* = 15.6 Hz), 6.71 (d, 2H, aromatic $H_3$, $H_5$, *J* = 8.8 Hz), 7.69 (d, 2H, aromatic $H_2$, $H_6$, *J* = 8.8 Hz). MS: *m/z* (%): 310 ($M^+$+2, 34%), 311 ($M^+$+3, 23%) and base peak at 282 (100%). Anal. Calcd for $C_{19}H_{20}N_2O_2$: C, 74.00; H, 6.54; N, 9.08. Found: C, 74.13; H, 6.41; N, 9.17.

*6.1.3.7. (E)-3-(4-(4-(4-Chlorophenyl)piperazin-1-yl)phenyl)acrylic acid* ***IIIg (E)***. Yield 95% as pale yellow solid, mp 201 °C. IR: (Ú max, $cm^{-1}$): 1594 (C=C), 1699 (C=O, COOH), 2918–3434 (OH, COOH). $^1$H NMR (300 MHz)(DMSO) δ: 3.23 (t, 4H, piperazine $H_3$, $H_5$, *J* = 4.5 Hz), 3.53 (t, 4H, piperazine $H_2$, $H_6$, *J* = 4.8 Hz), 6.32 (d, 1H, CH=C$\underline{H}$-COOH, *J* = 16.2 Hz), 7.02–7.13 (m, 4H, aromatic $H_3$,

$H_5$, $H_{2'}$, $H_{6'}$), 7.48 (d, 1H, C<u>H</u>=CH—COOH, $J$ = 16.2 Hz), 6.7 (d, 2H, aromatic $H_{3'}$, $H_{5'}$, $J$ = 8.4 Hz), 7.82 (d, 2H, aromatic $H_2$, $H_6$). MS: *m/z* (%): 342 ($M^+$, 42%), 344 (M+2, 9%) and base peak at 64 (100%). Anal. Calcd for $C_{19}H_{19}ClN_2O_2$: C, 66.57; H, 5.59; N, 8.17. Found: C, 66.68; H, 5.64; N, 8.29.

*6.1.4. General method for preparation of 1-(substituted)-4-nitrobenzene* ***IVa,b,e,f*** *[34]*

A mixture of p-nitro chlorobenzene **3** (25.0 g, 0.200 mol), appropriate secondary amine **2a**,**b**,**e**,**f** (0.300 mol) and anhydrous potassium carbonate (40.0 g) were mixed in DMF (300 mL), and then catalytic drops of Aliquat 336 reagent were added. The mixture was heated from 24 to 36 h at 100 °C. The reaction mixture was then concentrated under vacuum, cooled and poured into ice water and left aside overnight. The formed solid was filtered, washed with water and crystallized from ethanol to yield titled compounds **IVa**,**b**,**e**,**f**.

*6.1.4.1. 1-(4-Nitrophenyl)-1H-imidazole* ***IVa***. Yield 65% as pale yellow solid, mp 203 °C, (as reported) [58,59].

*6.1.4.2. 1-(4-Nitrophenyl)pyrrolidine* ***IVb***. Yield 98% as orange solid, mp 169 °C, (as reported) [60,61].

*6.1.4.3. 1-Methyl-4-(4-nitrophenyl)piperazine* ***IVe***. Yield 98% as orange solid, mp 104 °C, (as reported) [62].

*6.1.4.4. 1-(4-Nitrophenyl)-4-phenylpiperazine* ***IVf***. Yield 92% as red solid, mp184 °C, (as reported) [63].

*6.1.5. General method for preparation of 4-(substituted)aniline* ***Va,b,e,f*** *[36,37]*

To a solution of 1-(substituted) 4-nitrobenzene **IVa**,**b**,**e**,**f** (0.01 mol) in $NH_4OH$ (20 mL, 30%), a solution of sodium dithionite (7 g, 0.04 mol) in water (30 mL) was quickly added, the reaction mixture was refluxed for 15 min. After cooling, the crude product was filtered, washed and crystallized from methylene chloride to yield target compounds **Va**,**b**,**e**,**f**.

*6.1.5.1. 4-(1H-imidazol-1-yl) aniline* ***Va***. Yield 70% as gray solid, mp 147 °C, (as reported) [64,65].

*6.1.5.2. 4-(Pyrrolidin-1-yl) aniline* ***Vb***. Yield 80% as yellow oil, (as reported) [66].

*6.1.5.3. 4-(4-Methylpiperazin-1-yl) aniline* ***Ve***. Yield 75% as off white acicular solid, mp 90 °C, (as reported) [62,67,68].

*6.1.5.4. 4-(4-Phenylpiperazin-1-yl) aniline* ***Vf***. Yield 80% as white solid, mp 128–130 °C, (as reported) [63].

*6.1.6. General method for preparation of 4-(4-(substituted)phenylamino)-4-oxobutanoic acid* ***VIa,b,e*** *[69]*

A mixture of 4-(substituted) aniline **Va**,**b**,**e** (0.003 mol) and succinic anhydride (0.30 g, 0.003 mol) were mixed in 10 (mL) methylene chloride as a solvent. The mixture was allowed to stir on cold for 24 h till the product is precipitated. The solid was then filtered, washed with methylene chloride and crystallized with diethyl ether to yield the required product **VIa**,**b**,**e**.

*6.1.6.1. 4-(4-(1H-imidazol-1-yl)phenylamino)-4-oxobutanoic acid* ***VIa***. Yield 98% as grayish white solid, mp 238 °C. IR: (Ú max, $cm^{-1}$): 1654 (C=O, amide), 1715 (C=O, COOH), 3295 (NH), 2965–3220 (OH, COOH). $^1$H NMR (400 MHz)(DMSO) δ: 2.56 (t, 2H, C<u>H</u>$_2$-C<u>H</u>$_2$COOH, $J$ = 5.4 Hz), 2.63 (t, 2H, CH$_2$C<u>H</u>$_2$COOH, $J$ = 5.5 Hz), 7.02 (s, 1H, imidazole $H_2$), 7.52 (d, 2H, aromatic $H_3$, $H_5$, $J$ = 8.2 Hz), 7.61 (d, 1H, imidazole $H_4$), 7.66 (d, 2H, aromatic $H_2$, $H_6$, $J$ = 8.2 Hz), 8.11 (d, 1H, imidazole $H_5$), 10.07 (s, 1H, N<u>H</u>), 12.08 ($s_{br}$, 1H, COO<u>H</u>). MS: *m/z* (%): 259 ($M^+$, 55%), 260 ($M^+$+1, 17%) and base peak at 157 (100%). Anal. Calcd for $C_{13}H_{13}N_3O_3$: C, 60.22; H, 5.05; N, 16.21. Found: C, 60.47; H, 5.11; N, 16.37.

*6.1.6.2. 4-(4-(Pyrrolidin-1-yl)phenylamino)-4-oxobutanoic acid* ***VIb***. Yield 87% as grayish white solid, mp 195 °C. IR: (Ú max, $cm^{-1}$): 1652 (C=O, amide), 1713 (C=O, COOH), 3290 (NH), 2839–3115 (OH, COOH). $^1$H NMR (300 MHz)(DMSO) δ: 1.91–1.95 (m, 4H, pyrrolidine $H_3$, $H_4$), 2.48–2.62 (m, 4H, C<u>H</u>$_2$C<u>H</u>$_2$COOH), 3.19 (t, 4H, pyrrolidine $H_2$, $H_5$, $J$ = 6.3 Hz), 6.48 (d, 2H, aromatic $H_3$, $H_5$, $J$ = 8 Hz), 7.37 (d, 2H, aromatic $H_2$, $H_6$, $J$ = 8.7 Hz), 9.58 (s, 1H, N<u>H</u>), 12.00 ($s_{br}$, 1H, COO<u>H</u>). MS: *m/z* (%): 262 ($M^+$, 48%), 263 ($M^+$+1, 26%) and base peak at 161 (100%). Anal. Calcd for $C_{14}H_{18}N_2O_3$: C, 64.10; H, 6.92; N, 10.68. Found: C, 64.23; H, 7.01; N, 10.81.

*6.1.6.3. 4-(4-(4-Methylpiperazin-1-yl)phenylamino)-4-oxobutanoic acid* ***VIe***. Yield 85% as grayish white solid, mp 168 °C. IR: (Ú max, $cm^{-1}$): 1659 (C=O, amide), 1710 (C=O, COOH), 3297 (NH), 2954–3212 (OH, COOH). $^1$H NMR (400 MHz)(DMSO) δ: 2.19 (t, 4H, piperazine $H_3$, $H_5$), 2.34 (s, 3H, $CH_3$-piperazine), 2.44 (t, 2H, C<u>H</u>$_2$CH$_2$COOH, $J$ = 6.6 Hz), 2.99 (t, 2H, CH$_2$C<u>H</u>$_2$COOH, $J$ = 6.6 Hz), 3.34 (t, 4H, piperazine $H_2$, $H_6$), 6.81 (d, 2H, aromatic $H_3$, $H_5$, $J$ = 8.8 Hz), 7.36 (d, 2H, aromatic $H_2$, $H_6$, $J$ = 8.8 Hz), 9.65 (s, 1H, N<u>H</u>). MS: *m/z* (%): 291 ($M^+$, 38%), 292 ($M^+$+1, 12%) and base peak at 189 (100%). Anal. Calcd for $C_{15}H_{21}N_3O_3$: C, 61.84; H, 7.27; N, 14.42. Found: C, 62.01; H, 7.36; N, 14.65.

*6.1.7. General method for preparation of 5-(4-(substituted)phenylamino)-5-oxopentanoic acid* ***VIIa,f*** *[70]*

A mixture of 4 (substituted) aniline **Va**,**f** (0.003 mol) and glutaric anhydride (0.34 g, 0.003 mol) were dissolved in (10 mL) methylene chloride. The solution was allowed to stir on cold for 24 h till the product is precipitated. The solid was then filtered, washed with methylene chloride and crystallized with diethyl ether to yield the required product **VIIa**,**f**.

*6.1.7.1. 5-(4-(1H-imidazol-1-yl)phenylamino)-5-oxopentanoic acid* ***VIIa***. Yield 90% as grayish white solid, mp 230 °C.IR: (Ú max, $cm^{-1}$): 1659 (C=O, amide), 1708 (C=O, COOH), 3295 (NH), 2899–3186 (OH, COOH). $^1$H NMR (400 MHz)(DMSO) δ: 1.78 (t, 2H, CH$_2$—C<u>H</u>$_2$—CH$_2$—COOH, $J$ = 7.2 Hz), 2.24 (t, 2H, CH$_2$—CH$_2$—C<u>H</u>$_2$—COOH, $J$ = 7.2 Hz), 2.30 (t, 2H, C<u>H</u>$_2$—CH$_2$—CH$_2$—COOH, $J$ = 7.2 Hz), 7.02 (s, 1H, imidazole $H_2$), 7.49 (d, 2H, aromatic $H_3$, $H_5$, $J$ = 8.8 Hz), 7.61 (d, 1H, imidazole $H_4$), 7.64 (d, 2H, aromatic $H_2$, $H_6$, $J$ = 8.8 Hz), 8.11 (d, 1H, imidazole $H_5$), 10.00 (s, 1H, N<u>H</u>), 12.04 ($s_{br}$, 1H, COO<u>H</u>). MS: *m/z* (%): 273 ($M^+$, 49%), 274 ($M^+$+1, 18%) and base peak at 84 (100%). Anal. Calcd for $C_{14}H_{15}N_3O_3$: C, 61.53; H, 5.53; N, 15.38. Found: C, 61.76; H, 5.59; N, 15.52.

*6.1.7.2. 5-(4-(4-Phenylpiperazin-1-yl)phenylamino)-5-oxopentanoic acid* ***VIIf***. Yield 95% as grayish white solid, mp 223 °C. IR: (Ú max, $cm^{-1}$): 1653 (C=O, amide), 1701 (C=O, COOH), 3291 (NH), 2962–3181 (OH, COOH). $^1$H NMR (300 MHz)(DMSO) δ: 1.77–1.82 (t, 2H, CH$_2$—C<u>H</u>$_2$—CH$_2$—COOH, $J$ = 7.2 Hz), 2.24–2.33 (m, 4H, C<u>H</u>$_2$—CH$_2$—C<u>H</u>$_2$—COOH), 3.20–3.27 (m, 8H, piperazine), 6.78 (t, 1H, aromatic $H_{4'}$, $J$ = 7.2 Hz), 6.92 (d, 2H, aromatic $H_3$, $H_5$, $J$ = 8 Hz), 7.01 (d, 2H, aromatic $H_{2'}$, $H_{6'}$, $J$ = 8.1 Hz), 7.26 (d, 2H, aromatic $H_{3'}$, $H_{5'}$, $J$ = 7.2 Hz), 7.44 (d, 2H, aromatic $H_2$, $H_6$, $J$ = 8 Hz), 9.69 (s, 1H, N<u>H</u>), 12.00 ($s_{br}$, 1H, COO<u>H</u>). MS: *m/z* (%): 367 ($M^+$, 37%), 368 ($M^+$+1, 29%) and base peak at 80 (100%). Anal. Calcd for $C_{21}H_{25}N_3O_3$: C, 68.64; H, 6.86; N, 11.44. Found: C, 68.78; H, 6.56; N, 11.59.

*6.1.8. General method for the preparation of 2-((4-substituted)phenyl)carbamoyl) benzoic acid* ***VIIIa,e*** *[71]*

A mixture of 4 (substituted) aniline **Va**,**e** (0.003 mol) and phthalic anhydride (0.44 g, 0.003 mol) were dissolved in (10 mL) methylene chloride. The solution was allowed to stir on cold for 24 h till the product is precipitated. The solid was then filtered, washed with methylene chloride and crystallized with diethyl ether to yield the required product **VIIIa**,**e**.

*6.1.8.1. 2-((4-(1H-Imidazol-1-yl)phenyl)carbamoyl) benzoic acid* ***VIIIa***. Yield 95% as grayish white solid, mp 264 °C. IR: (Ú max, $cm^{-1}$): 1659 (C=O, amide), 1711 (C=O, COOH), 3295 (NH), 2972–3214 (OH, COOH). $^1$H NMR (400 MHz)(DMSO) δ: 7.06 (s, 1H, imidazole $H_2$), 7.50–7.63 (m, 4 H, phthalic), 7.57 (d, 2H, aromatic $H_3$, $H_5$, $J$ = 8.8 Hz), 7.65 (d, 1H, imidazole $H_4$), 7.76 (d, 2H, aromatic $H_2$, $H_6$, $J$ = 8.8 Hz), 8.17 (d, 1H, imidazole $H_5$), 10.43 (s, 1H, NH). MS: *m/z* (%): 307 ($M^+$, 55%), 308 ($M^+$+1, 17%) and base peak at 121 (100%). Anal. Calcd for $C_{17}H_{13}N_3O_3$: C, 66.44; H, 4.26; N, 13.67. Found: C, 66.6; H, 4.32; N, 13.79.

*6.1.8.2. 2-((4-(4-Methylpiperazin-1-yl)phenyl)carbamoyl) benzoic acid* ***VIIIe***. Yield 89% as off white solid, mp 192.5 °C. IR: (Ú max, $cm^{-1}$): 1650 (C=O, amide), 1702 (C=O, COOH), 3298 (NH), 2994–3221 (OH, COOH). $^1$H NMR (400 MHz)(DMSO) δ: 1.95 (t, 4H, piperazine $H_3$, $H_5$), 2.30 (s, 3H, $CH_3$-piperazine), 3.22 (t, 4H, piperazine $H_3$, $H_5$), 6.91 (d, 2H, aromatic $H_3$, $H_5$, $J$ = 8.8 Hz), 7.46 (d, 2H, aromatic $H_2$, $H_6$, $J$ = 8.8 Hz), 7.44–7.60 (m, 4H, phthalic), 10.09 (s, 1H, NH). MS: *m/z* (%): 339 ($M^+$, 60%), 340 ($M^+$+1, 28%) and base peak at 189 (100%). Anal. Calcd for $C_{19}H_{21}N_3O_3$: C, 67.24; H, 6.24; N, 12.38. Found: C, 67.38; H, 6.29; N, 12.51.

*6.2. Cell growth inhibitory activity in cancer cells*

*6.2.1. Evaluation for cytotoxic activity against a panel of sixty human cancer cell lines*

National Cancer Institute (NCI) for *in vitro* anticancer assay evaluates different compounds for their anticancer activity. The screening is a two-stage process, beginning with the evaluation of all compounds against the full NCI 60 cell lines panel representing Leukemia, Non-Small Cell Lung Cancer, Melanoma, colon cancer, CNS cancer, breast cancer, ovarian cancer, renal cancer and prostate cancer at a single dose of $10^{-5}$ M. The output from the single dose screen is reported as a mean graph and is available for analysis by the COMPARE program. Compounds which are selected are evaluated against the 60 cell panel at five concentration levels.

*6.2.1.1. Assay protocol.* Methodology of assay is as reported [72,73]. The human tumor cell lines of the cancer-screening panel are grown in RPMI 1640 medium containing 5% fetal bovine serum and 2 mM L-glutamine. For a typical screening experiment, cells are inoculated into 96 well microtiter plates in 100 ml at plating densities ranging from 5000 to 40,000 cells/well depending on the doubling time of individual cell lines. After cell inoculation, the microtiter plates are incubated at 37 °C, 5% $CO_2$, 95% air and 100% relative humidity for 24 h prior to addition of experimental drugs. After 24 h, two plates of each cell line are fixed in situ with TCA, to represent a measurement of the cell population for each cell line at the time of drug addition (Tz). Experimental drugs are solubilized in dimethyl sulfoxide at 400-fold the desired final maximum test concentration and stored frozen prior to use. At the time of drug addition, an aliquot of frozen concentrate is thawed and diluted to twice the desired final maximum test concentration with complete medium containing 50 mg/ml Gentamicin. Additional four, 10-fold or ½log serial dilutions are made to provide a total of five drug concentrations plus control. Aliquots of 100 ml of these different drug dilutions are added to the appropriate microtiter wells already containing 100 ml of medium, resulting in the required final drug concentrations. Following drug addition, the plates are incubated for an additional 48 h at 37 °C, 5% $CO_2$, 95% air, and 100% relative humidity. For adherent cells, the assay is terminated by the addition of cold TCA. Cells are fixed in situ by the gentle addition of 50 ml of cold 50% (w/v) TCA (final concentration, 10% TCA) and incubated for 60 min at 4 °C. The supernatant is discarded, and the plates are washed five times with tap water and air dried. Sulforhodamine B (SRB) solution (100 ml) at 0.4% (w/v) in 1% acetic acid is added to each well, and plates are incubated for 10 min at room temperature. After staining, unbound dye is removed by washing five times with 1% acetic acid and the plates are air dried. Bound stain is subsequently solubilized with 10 mM trizma base, and the absorbance is read on an automated plate reader at a wavelength of 515 nm. For suspension cells, the methodology is the same except that the assay is terminated by fixing settled cells at the bottom of the wells by gently adding 50 ml of 80% TCA (final concentration, 16% TCA).

*6.2.1.2. Data analysis.* Using the seven absorbance measurements [time zero, (Tz), control growth, (C), and test growth in the presence of drug at the five concentration levels (Ti)], the percentage growth is calculated at each of the drug concentrations levels. Percentage growth inhibition is calculated as: [(Ti – Tz)/(C – Tz)] – 100 for concentrations for which Ti > /¼ Tz and [(Ti – Tz)/Tz] – 100 for concentrations for which Ti < Tz: three dose response parameters are calculated for each experimental agent [74].

*6.2.2. Evaluation for cytotoxicity against HepG2 Cancer cell line*

*6.2.2.1. Cell culture.* HepG2 human hepatocellular carcinoma cells were grown in RPMI-1640 medium, supplemented with 10% heat inactivated FBS, 50 units/mL of penicillin and 50 mg/mL of streptomycin and maintained at 37° in a humidified atmosphere containing 5% $CO_2$. The cells were maintained as "monolayer culture" by serial subculturing.

*6.2.2.2. SRB cytotoxicity assay.* Cytotoxicity was determined using SRB method as previously described by Skehan et al. [75]. Exponentially growing cells were collected using 0.25% Trypsin–EDTA and seeded in 96-well plates at 1000–2000 cells/well in RPMI-1640 supplemented medium. After 24 h, cells were incubated for 72 h with various concentrations of the tested compounds. Following 72 h treatment, the cells will be fixed with 10% trichloroacetic acid for 1 h at 4 °C. Wells were stained for 10 min at room temperature with 0.4% SRB dissolved in 1% acetic acid. The plates were air dried for 24 h and the dye was solubilized with Tris–HCl for 5 min on a shaker at 1600 rpm. The optical density (OD) of each well was measured spectrophotometrically at 564 nm with an ELISA microplate reader (ChroMate-4300, FL, USA).

*6.2.3. Data analysis*

The $IC_{50}$ values were calculated according to the equation for Boltzmann sigmoidal concentration–response curve using the nonlinear regression fitting models (Graph Pad, Prism Version 5).

*6.3. Histone deacetylase inhibitory activity*

*6.3.1. Materials and methods*

The histone deacetylase activity was carried out by BPS Bioscience (www.bpsbioscience.com). Single dose concentration of 10 μM HDAC substrate 3 (BPS#50037) of HDAC1 (BPS#50051), HDAC2 (BPS#50002), HDAC3 (BPS#50003), HDAC6 (BPS#50006) and HDAC10 (BPS#50010) was used in testing. And also it was carried on 2 μM HDAC substrate 1 (BPS#50040) of HDAC4 (BPS#50004), HDAC5 (BPS#50005), HDAC7 (BPS#50007), HDAC8

(BPS#50008), HDAC9 (BPS#50009) and HDAC11 (BPS#50021). Other materials are used as HDAC Assay Buffer (BPS#50031), HDAC Assay Developer (BPS#50030), SAHA as a reference compound purchased from sigma (St. Louis, MO #SML0061) and TSN as another reference compound purchased from Selleckcom.com (#S1045).

*6.3.2. Assay protocols*

*6.3.2.1. In vitro HDAC1 inhibitory assay.* A 100 μM solution of each compound was prepared with 10% DMSO in HDAC assay buffer and 5 μl of the dilution was added to a 50 μl reaction so that the final concentration of DMSO is 1% in all of reactions. The enzymatic reactions for the HDAC enzymes were conducted in duplicate at 37 °C for 30 min in a 50 μl mixture containing HDAC assay buffer, 5 μg BSA, HDAC substrate 3, HDAC1 enzyme and a test compound (10 μM). After enzymatic reactions, 50 μl of 2 × HDAC Developer was added to each well for the HDAC enzymes and the plate was incubated at room temperature for an additional 15 min. Fluorescence intensity was measured at an excitation of 360 nm and an emission of 460 nm using a Tecan Infinite M1000 microplate reader.

*6.3.2.2. In vitro HDAC2–11 inhibitory assay.* A 500 μM solution of each compound was prepared with 10% DMSO in HDAC assay buffer and 5 μl of the dilution was added to a 50 μl reaction so that the final concentration of DMSO is 1% in all of reactions. The enzymatic reactions for the HDAC enzymes were conducted in duplicate at 37 °C for 30 min in a 50 μl mixture containing HDAC assay buffer, 5 μg BSA, HDAC substrate 1/3, a HDAC 2–11 enzyme and a test compound (50 μM). After enzymatic reactions, 50 μl of 2 × HDAC Developer was added to each well for the HDAC enzymes and the plate was incubated at room temperature for an additional 15 min. Fluorescence intensity was measured at an excitation of 360 nm and an emission of 460 nm using a Tecan Infinite M1000 microplate reader.

*6.3.3. Data analysis*

HDAC activity assays were performed in duplicates at each compound. The fluorescent intensity data were analyzed using the computer software, Graphpad Prism. In the absence of the compound, the fluorescent intensity ($F_t$) in each data set was defined as 100% activity. In the absence of HDAC, the fluorescent intensity ($F_b$) in each data set was defined as 0% activity. The percent activity in the presence of each compound was calculated according to the following equation: % activity = $(F - F_b)/(F_t - F_b)$, where $F$ = the fluorescent intensity in the presence of the compound.% Inhibition was calculated as: % inhibition = 100 (%)_% activity.

## Acknowledgments

The authors are grateful to The National Cancer Institute, Maryland, USA for performing anticancer activity and would like to thank BPS Bioscience for HDAC inhibition activity. And also would like to thank Dr. Ahmed Essmat (Pharmacology & Toxicology Department, Faculty of Pharmacy, AinShams University, Cairo, Egypt 11566) for performing the *in vitro* cytotoxicity assays against Liver HepG2 Cancer cell line.

## References

[1] W.D. Cress, E. Seto, J. Cell. Physiol. 184 (2000) 1–16.
[2] B.D. Strahl, C.D. Allis, Nature 403 (2000) 41–45.
[3] V. Morales, H. Richard-Foy, Mol. Cell. Biol. 20 (2000) 7230–7237.
[4] K. Struhl, Genes Dev. 12 (1998) 599–606.
[5] P.A. Wade, Hum. Mol. Genet. 10 (2001) 693–698.
[6] A.J. de Ruijter, A.H. van Gennip, H.N. Caron, S. Kemp, A.B. van Kuilenburg, Biochem. J. 370 (2003) 737–749.
[7] C. Hildmann, D. Riester, A. Schwienhorst, Appl. Microbiol. Biotechnol. 75 (2007) 487–497.
[8] D.C. Drummond, C.O. Noble, D.B. Kirpotin, Z. Guo, G.K. Scott, C.C. Benz, Annu. Rev. Pharmacol. Toxicol. 45 (2005) 495–528.
[9] H. Lu, Y. Chen, B. Yang, Q. You, Acta Pharma. Sin. B 1 (2011) 240–247.
[10] A. Vannini, C. Volpari, P. Gallinari, P. Jones, M. Mattu, A. Carfi, R. De Francesco, C. Steinkuhler, S. Di Marco, EMBO Rep. 8 (2007) 879–884.
[11] K.B. Glaser, Biochem. Pharmacol. 74 (2007) 659–671.
[12] M. Dokmanovic, P.A. Marks, J. Cell. Biochem. 96 (2005) 293–304.
[13] S. Ropero, M. Esteller, Mol. Oncol. 1 (2007) 19–25.
[14] M. Duvic, R. Talpur, X. Ni, C. Zhang, P. Hazarika, C. Kelly, J.H. Chiao, J.F. Reilly, J.L. Ricker, V.M. Richon, S.R. Frankel, Blood 109 (2007) 31–39.
[15] P.A. Marks, R. Breslow, Nat. Biotechnol. 25 (2007) 84–90.
[16] X. Kong, Z. Lin, D. Liang, D. Fath, N. Sang, J. Caro, Mol. Cell. Biol. 26 (2006) 2019–2028.
[17] A. Grassadonia, P. Cioffi, F. Simiele, L. Iezzi, M. Zilli, C. Natoli, Cancers (Basel) 5 (2013) 919–942.
[18] B. Venugopal, T.R. Evans, Curr. Med. Chem. 18 (2011) 1658–1671.
[19] O. Moradei, C.R. Maroun, I. Paquin, A. Vaisburg, Curr. Med. Chem. Anticancer Agents 5 (2005) 529–560.
[20] J.E. Bolden, M.J. Peart, R.W. Johnstone, Nat. Rev. Drug Discov. 5 (2006) 769–784.
[21] F. Wang, W. Lu, T. Zhang, J. Dong, H. Gao, P. Li, S. Wang, J. Bioorg. Med. Chem. 21 (2013) 6973–6980.
[22] T.A. Miller, D.J. Witter, S. J. Med. Chem. 46 (2003) 5097–5116.
[23] M.S. Finnin, J.R. Donigian, A. Cohen, V.M. Richon, R.A. Rifkind, P.A. Marks, R. Breslow, N.P. Pavletich, Nature 401 (1999) 188–193.
[24] Y.D. Chen, Y.J. Jiang, J.W. Zhou, Q.S. Yu, Q.D. You, J. Mol. Graph. Model 26 (2008) 1160–1168.
[25] M. Jung, G. Brosch, D. Kolle, H. Scherf, C. Gerhauser, P. Loidl, J. Med. Chem. 42 (1999) 4669–4679.
[26] S.M. Sternson, J.C. Wong, C.M. Grozinger, S.L. Schreiber, Org. Lett. 3 (2001) 4239–4242.
[27] B. Gopalan, T. Ponpandian, V. Kachhadia, K. Bharathimohan, R. Vignesh, V. Sivasudar, S. Narayanan, B. Mandar, R. Praveen, N. Saranya, S. Rajagopal, S. Rajagopal, Bioorg. Med. Chem. Lett. 23 (2013) 2532–2537.
[28] A.V. Bieliauskas, S.V. Weerasinghe, M.K. Pflum, Bioorg. Med. Chem. Lett. 17 (2007) 2216–2219.
[29] E. Hahnen, J. Hauke, C. Trankle, I.Y. Eyupoglu, B. Wirth, I. Blumcke, Drugs 17 (2008) 169–184.
[30] G. Bora-Tatar, D. Dayangac-Erden, A.S. Demir, S. Dalkara, K. Yelekci, H. Erdem-Yurter, Bioorg. Med. Chem. 17 (2009) 5219–5228.
[31] J.S. Chen, D.V. Faller, R.A. Spanjaard, Curr. Cancer Drug Targets 3 (2003) 219–236.
[32] M. Gottlicher, S. Minucci, P. Zhu, O.H. Kramer, A. Schimpf, S. Giavara, J.P. Sleeman, F. Lo Coco, C. Nervi, P.G. Pelicci, T. Heinzel, EMBO J. 20 (2001) 6969–6978.
[33] J. Pearn, Lancet 1 (1980) 919–922.
[34] Z.Q. Liang, C.X. Wang, J.X. Yang, H.W. Gao, Y.P. Tian, X.T. Tao, M.H. Jiang, New J. Chem. 31 (2007) 906–910.
[35] K. Abouzid, P. Frohberg, J. Lehmann, M. Decker, Med. Chem. 3 (2007) 433–438.
[36] S. Mowafy, N.A. Farag, K.A.M. Abouzid, Eur. J. Med. Chem. 61 (2013) 132–145.
[37] H.A.A. Shady, S.L. El-Ansary, D.A.A. El-Ella, N.A. Farag, Bull. Fac. Pharm. Cairo Univ. 42 (2004) 31–42.
[38] S. Ray, C. Lee, T. Hou, I. Boldogh, A.R. Brasier, Nucleic Acids Res. 36 (2008) 4510–4520.
[39] H. Su, A. Nebbioso, V. Carafa, Y. Chen, B. Yang, L. Altucci, Q. You, Bioorg. Med. Chem 16 (2008) 7992–8002.
[40] H. Li, J. Sutter, R. Hoffmann, HypoGen: an automated system for generating predictive 3D pharmacophore models, in: O.F. Güner (Ed.), Pharmacophore Perception, Development, and use in Drug Design, International University Line, La Jolla, CA, 2000, pp. 171–187.
[41] R.F. George, N.S.M. Ismail, J. Stawinski, A.S. Girgis Eur, J. Med. Chem. 68 (2013) 339–351.
[42] A.S. Girgis, J. Stawinski, N.S.M. Ismail, H. Farag, Eur J. Med. Chem. 47 (2012) 312–322.
[43] A.K. Ghose, G.M. Crippen, J. Comput. Chem. 7 (1986) 565–577.
[44] L. Zhu, G. Li, L. Luo, P. Guo, J. Lan, J. You, J. Org. Chem. 74 (2009) 2200–2202.
[45] D. Kumar, K.K. Raj, M. Bailey, T. Alling, T. Parish, D.S. Rawat, Bioorg. Med. Chem. Lett. 23 (2013) 1365–1369.
[46] M. Sarma, T. Chatterjee, S. Ghanta, S.K. Das, J. Org. Chem. 77 (2012) 432–444.
[47] N.R. Eibergen, I. Im, N.Y. Patel, P. Hergenrother, J. Chembiochem, Eur. J. Chem. Biol. 13 (2012) 574–584.
[48] P.G. Mandhane, R.S. Joshi, D.R. Nagargoje, A.V. Chate, C.H. Gill, Sulfur Silicon Relat. Elem. 186 (2010) 149–158.
[49] R.S. Joshi, P.G. Mandhane, S.D. Diwakar, S.K. Dabhade, C.H. Gill, Bioorg. Med. Chem. Lett. 20 (2010) 3721–3725.
[50] M. Meciarova, S. Toma, P. Magdolen, Ultrason. Sonochem. 10 (2003) 265–270.
[51] S. Lieber, F. Scheer, W. Meissner, S. Naruhn, T. Adhikary, S. Muller-Brusselbach, W.E. Diederich, R. Muller, J. Med. Chem. 55 (2012) 2858–2868.
[52] L. Heping, G. Cancheng, R. Jianming, H. Boyun, J. Org. Chem. 24 (2004) 783–787.
[53] S.R. Byeon, Y.J. Jin, S.J. Lim, J.H. Lee, K.H. Yoo, K.J. Shin, S.J. Oh, D. Kim, J. Bioorg. Med. Chem. Lett. 17 (2007) 4022–4025.
[54] A. Bombrun, U.S. Patent 6, 306, 870B1, 2001.
[55] I. Sircar, B.L. Duell, J.A. Bristol, R.E. Weishaar, D.B. Evans, J. Med. Chem. 30 (1987) 1023–1029.

[56] S. Sasmal, D. Balasubrahmanyam, H.R. Kanna Reddy, G. Balaji, G. Srinivas, S. Cheera, C. Abbineni, P.K. Sasmal, I. Khanna, V.J. Sebastian, V.P. Jadhav, M.P. Singh, R. Talwar, J. Suresh, D. Shashikumar, K. Harinder Reddy, V. Sihorkar, T.M. Frimurer, O. Rist, L. Elster, T. Hogberg, Bioorg. Med. Chem. Lett. 22 (2012) 3163–3167.
[57] J. Guo, W. Dong, W. Liu, Z. Yan, N. Wang, Z. Liu, Eur J. Med. Chem. 62 (2013) 670–676.
[58] K. Yang, Y. Qiu, Z. Li, Z. Wang, S. Jiang, J. Org. Chem. 76 (2011) 3151–3159.
[59] Q. Zhang, J. Luo, Y. Wei, Synth. Commun. 42 (2011) 114–121.
[60] R.N. Prabhu, R. Ramesh, Tetrahedron Lett. 54 (2013) 1120–1124.
[61] B. Sreedhar, R. Arundhathi, P.L. Reddy, M.L. Kantam, J. Org. Chem. 74 (2009) 7951–7954.
[62] M.I. Husain, S.K. Agarwal, Ind. J. Chem. 13 (1975) 1238–1239.
[63] M. Khatri, S.K. Rai, S. Alam, A. Vij, M. Tiwari, Bioorg. Med. Chem. 17 (2009) 1890–1897.
[64] J.M. Smallheer, R.S. Alexander, J. Wang, S. Wang, S. Nakajima, K.A. Rossi, A. Smallwood, F. Barbera, D. Burdick, J.M. Luettgen, R.M. Knabb, R.R. Wexler, P.K. Jadhav, Bioorg. Med. Chem. Lett. 14 (2004) 5263–5267.
[65] J. Engel-Andreasen, B. Shimpukade, T. Ulven, Green Chem. 15 (2013) 336–340.
[66] S.K. Singh, M. Srinivasa Reddy, M. Mangle, K. Ravi Ganesh, Tetrahedron 63 (2007) 126–130.
[67] P. Xiang, T. Zhou, L. Wang, C.Y. Sun, J. Hu, Y.L. Zhao, L. Yang, Molecules 17 (2012) 873–883.
[68] A.D. Desai, K.H. Chikhalia, E-J. Chem. 2 (2005) 15–20.
[69] Y. Liu, L. Shang, H. Fang, H. Zhu, J. Mu, Q. Wang, X. Wang, Y. Yuan, W. Xu, Bioorg. Med. Chem. 17 (2009) 7398–7404.
[70] Y. Xu, N. Yamamoto, D.I. Ruiz, D.S. Kubitz, K.D. Janda, Bioorg. Med. Chem. Lett. 15 (2005) 4304–4307.
[71] A.M. Granados, R.H. de Rossi, J. Org. Chem. 66 (2001) 1548–1552.
[72] R.H. Shoemaker, Nat. Rev. Cancer 6 (2006) 813–823.
[73] M.R. Grever, S.A. Schepartz, B.A. Chabner, Semin. Oncol. 19 (1992) 622–638.
[74] M.C. Alley, D.A. Scudiero, A. Monks, M.L. Hursey, M.J. Czerwinski, D.L. Fine, B.J. Abbott, J.G. Mayo, R.H. Shoemaker, M.R. Boyd, Cancer Res. 48 (1988) 589–601.
[75] P. Skehan, R. Storeng, D. Scudiero, A. Monks, J. McMahon, D. Vistica, J.T. Warren, H. Bokesch, S. Kenney, M.R. Boyd, J. Natl. Cancer Inst. 82 (1990) 1107–1112.